12-2014

Holocene Earthquakes and Right-lateral Slip on the Left-lateral Darrington-Devils Mountain Fault Zone, Northern Puget Sound, Washington

Stephen F. Personius

Richard W. Briggs

Alan R. Nelson

Elizabeth R. Schermer
Western Washington University, liz.schermer@wwu.edu

J. Zebulon Maharrey
University of Alaska, Fairbanks

See next page for additional authors

Recommended Citation

Authors

Stephen F. Personius, Richard W. Briggs, Alan R. Nelson, Elizabeth R. Schermer, J. Zebulon Maharrey, Brian L. Sherrod, Sarah A. Spaulding, and Lee-Ann Bradley

Holocene earthquakes and right-lateral slip on the left-lateral Darrington–Devils Mountain fault zone, northern Puget Sound, Washington

Stephen F. Personius[1,*], Richard W. Briggs[1,*], Alan R. Nelson[1,*], Elizabeth R. Schermer[2,*], J. Zebulon Maharrey[1,3,*], Brian L. Sherrod[4,*], Sarah A. Spaulding[5,*], and Lee-Ann Bradley[1,*]

[1]*Geologic Hazards Science Center, U.S. Geological Survey, MS 966, P.O. Box 25046, Denver, Colorado 80225, USA*
[2]*Geology Department, Western Washington University, 516 High Street, Bellingham, Washington 98225-9080, USA*
[3]*Department of Geology and Geophysics, University of Alaska, Fairbanks, 900 Yukon Drive, P.O. Box 755780, Fairbanks, Alaska 99775, USA*
[4]*U.S. Geological Survey at Department of Geological Sciences, University of Washington, Box 351310, Seattle, Washington 98195, USA*
[5]*U.S. Geological Survey at INSTAAR, 1560 30th Street, Boulder, Colorado 80309, USA*

ABSTRACT

Sources of seismic hazard in the Puget Sound region of northwestern Washington include deep earthquakes associated with the Cascadia subduction zone, and shallow earthquakes associated with some of the numerous crustal (upper-plate) faults that crisscross the region. Our paleoseismic investigations on one of the more prominent crustal faults, the Darrington–Devils Mountain fault zone, included trenching of fault scarps developed on latest Pleistocene glacial sediments and analysis of cores from an adjacent wetland near Lake Creek, 14 km southeast of Mount Vernon, Washington. Trench excavations revealed evidence of a single earthquake, radiocarbon dated to ca. 2 ka, but extensive burrowing and root mixing of sediments within 50–100 cm of the ground surface may have destroyed evidence of other earthquakes. Cores in a small wetland adjacent to our trench site provided stratigraphic evidence (formation of a laterally extensive, prograding wedge of hillslope colluvium) of an earthquake ca. 2 ka, which we interpret to be the same earthquake documented in the trenches. A similar colluvial wedge lower in the wetland section provides possible evidence for a second earthquake dated to ca. 8 ka. Three-dimensional trenching techniques revealed evidence for 2.2 ± 1.1 m of right-lateral offset of a glacial outwash chan-

nel margin, and 45–70 cm of north-side-up vertical separation across the fault zone. These offsets indicate a net slip vector of 2.3 ± 1.1 m, plunging 14° west on a 286°-striking, 90°-dipping fault plane. The dominant right-lateral sense of slip is supported by the presence of numerous Riedel R shears preserved in two of our trenches, and probable right-lateral offset of a distinctive bedrock fault zone in a third trench. Holocene north-side-up, right-lateral oblique slip is opposite the south-side-up, left-lateral oblique sense of slip inferred from geologic mapping of Eocene and older rocks along the fault zone. The cause of this slip reversal is unknown but may be related to clockwise rotation of the Darrington–Devils Mountain fault zone into a position more favorable to right-lateral slip in the modern N-S compressional stress field.

INTRODUCTION

The Cascadia subduction zone is the dominant source of seismic hazard in the Puget Sound region of northwestern Washington (e.g., Petersen et al., 2008), but additional seismic sources related to crustal (upper-plate) faults in the forearc of the subduction zone have been identified in the last decade (Fig. 1) through the acquisition and analysis of high-resolution light detection and ranging (LiDAR) data (e.g., Harding and Berghoff, 2000; Haugerud et al., 2003). The E-W to NW-SE strikes of most of these faults and the coincidence of some of these faults with the margins of similarly trending Tertiary basins and uplifts are thought to reflect the N-S compression caused by northward transport of the Oregon block against a backstop of quasi-stable crust in southern

British Columbia (Fig. 1A; Wells et al., 1998, 2014; Wells and Simpson, 2001; McCaffrey et al., 2007). From south to north, paleoseismic and geologic mapping studies have identified surface deformation indicating Holocene activity on the Olympia and Tacoma faults in the Tacoma Basin (Bucknam et al., 1992; Sherrod, 2001; Sherrod et al., 2004a, 2004b; Nelson et al., 2008; Barnett et al., 2010; Sherrod and Gomberg, 2014), the Seattle fault in the Seattle Basin (Bucknam et al., 1999; Johnson et al., 1999; Sherrod et al., 2000; Nelson et al., 2003a, 2003b, 2014; Kelsey et al., 2008), the Southern Whidbey Island, Utsalady Point, and Darrington–Devils Mountain faults in the Everett Basin (Johnson et al., 1996, 2001, 2004; Dragovich and DeOme, 2006; Sherrod et al., 2008), and the Boulder Creek, Birch Bay, Sandy Point, and Drayton Harbor faults in the Bellingham Basin (Kelsey et al., 2012; Sherrod et al., 2013; Sherrod and Gomberg, 2014). Other Holocene faults that lie outside of the margins of the Tertiary basins include the Lake Creek–Boundary Creek (Little River) fault and the Saddle Mountains fault zone, which form parts of the north and east flanks, respectively, of the uplifted Olympic Mountains (Wilson et al., 1979; Nelson et al., 2007; Walsh and Logan, 2007; Witter et al., 2008; Blakely et al., 2009; Sherrod and Gomberg, 2014). Shallow seismicity is associated with some of these structures but not others (Fig. 1B).

We focused our investigation on one of these crustal faults, the Darrington–Devils Mountain fault zone, because despite prior work indicating the likelihood of Holocene displacement, the late Quaternary paleoseismic history of this prominent structure was heretofore unknown. As currently mapped, the Darrington–Devils

*E-mails: Personius—personius@usgs.gov; Briggs—rbriggs@usgs.gov; Nelson—anelson@usgs.gov; Schermer—schermer@geol.wwu.edu; Maharrey—jzmaharrey@alaska.edu; Sherrod—bsherrod@usgs.gov; Spaulding—sspaulding@usgs.gov; Bradley—bradley@usgs.gov.

Figure 1. Tectonic setting of Puget Sound region and Darrington–Devils Mountain fault zone (DDMFZ). (A) Regional tectonic setting of Pacific Northwest modified from block rotation model of Wells et al. (1998). Abbreviations: JDF—Juan de Fuca plate, NAM—North American plate, and PAC—Pacific plate; B&R—Basin and Range, NCS—Northern Cascadia, ORC—Oregon Coast Range, SNV—Sierra Nevada, VOL—volcanic extensional, and YAK—Yakima fold belt blocks; SAF—San Andreas fault; CSZ—Cascadia subduction zone. Gray arrows show direction of modeled block rotations from McCaffrey et al. (2007). White arrows are plate motion directions and velocities (in mm/yr) relative to North America (Wells et al., 1998; McCaffrey et al., 2007). Location of "backstop" buttress and location of northern margin of Northern Cascadia forearc block are from Kelsey et al. (2012). (B) Locations of Holocene-active (red) and other (black) Quaternary faults, margins of Tertiary forearc basins, and shallow (<25 km) seismicity in Puget Lowland of northwest Washington. Fault traces are modified from Barnett et al. (2010), Kelsey et al. (2012), and Quaternary Fault and Fold Database of the United States (U.S. Geological Survey, 2013). Outlines of Tertiary basins (heavy pink lines) are modified from Brocher et al. (2001), Kelsey et al. (2012), and Mace and Keranen (2012). Abbreviations: BB—Bellingham, EB—Everett, SB—Seattle, and TB—Tacoma basins; KA—Kingston Arch, SU—Seattle uplift; BBF—Birch Bay, BCF—Boulder Creek, DHF—Drayton Harbor, LCF—Lake Creek, OF—Olympia, SF—Seattle, SMF—Saddle Mountain, SPF—Sandy Point, SWF—South Whidbey Island, TF—Tacoma, and UPF—Utsalady Point faults; DDMFZ—Darrington–Devils Mountain fault zone. Seismicity (orange circles) from ANSS (Advanced National Seismic System) catalog (M) ≥3.0, depth ≤25 km, 1900–2013 (http://earthquake.usgs.gov/earthquakes/search/, accessed 07 September 2013).
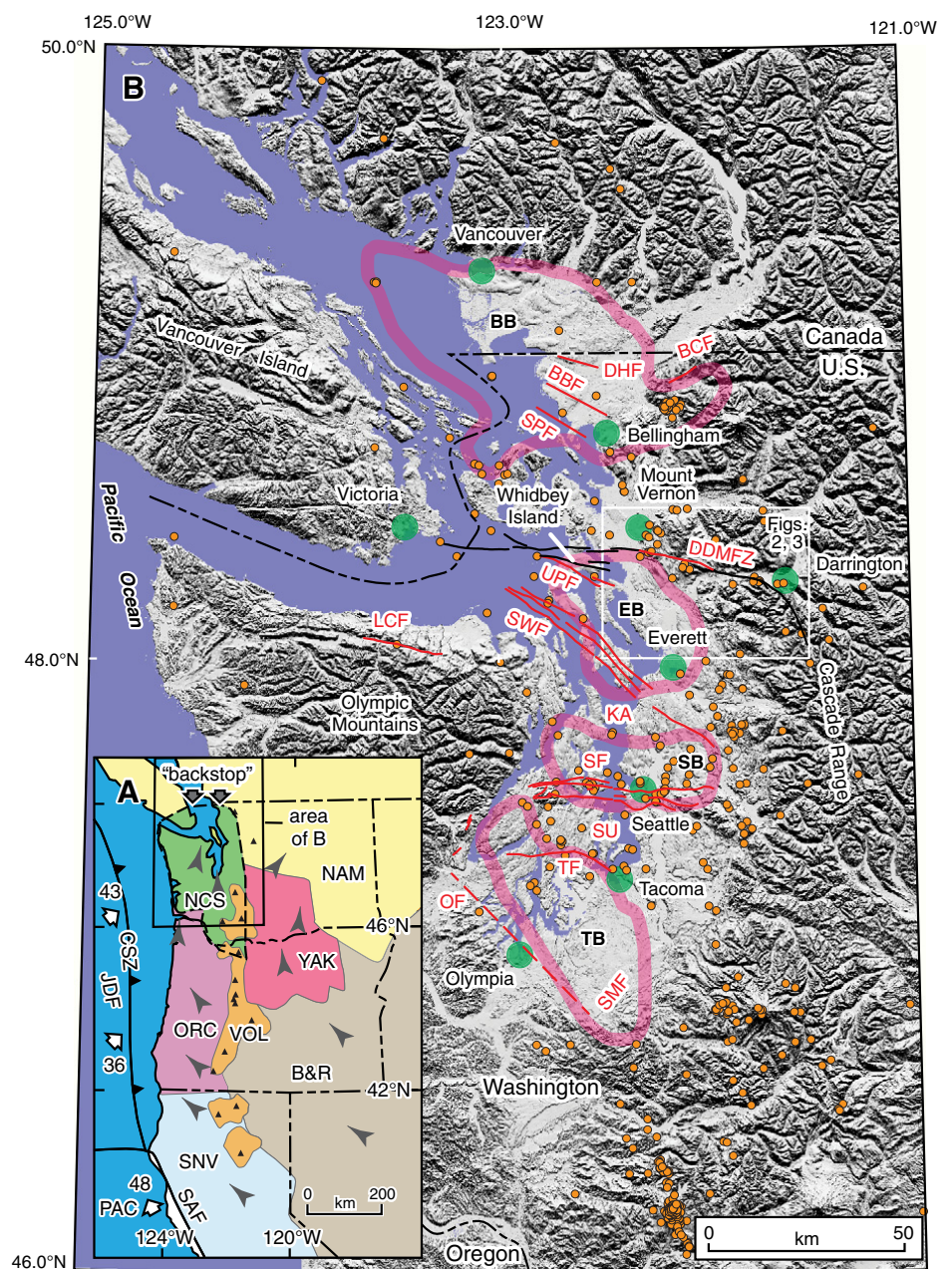

Mountain fault zone extends >125 km roughly E-W across the northern Puget Sound region, from near Victoria, British Columbia, eastward to south of Darrington, Washington, in the foothills of the North Cascades (Fig. 1B). The Darrington–Devils Mountain fault zone is thought to have formed in the early Eocene, and it juxtaposes Mesozoic accreted terranes (Trafton sequence, and Western and Eastern mélange belts) to the south against Upper Mesozoic terranes (Helena-Haystack mélange

and Easton metamorphic suite) to the north (Fig. 2; Whetten et al., 1988; Tabor, 1994; Johnson et al., 1996; Tabor et al., 2002; Dragovich and DeOme, 2006). In our area of investigation, the Darrington–Devils Mountain fault zone is coincident with the northern margin of the Tertiary Everett Basin, and it juxtaposes a thick section of Eocene to Oligocene continental sedimentary rocks (Rocks of Bulson Creek) to the south against similar Eocene rocks (Chuckanut Formation) to the north. Less-extensive out-

crops of Eocene intrusive and extrusive igneous rocks are localized along the Darrington–Devils Mountain fault zone and other structures in the area (Dragovich and DeOme, 2006). The Darrington–Devils Mountain fault zone has had a long (~50 m.y.) and complicated slip history, which may have included an early period of right-lateral oblique slip (Tabor, 1994). Numerous NW-striking en echelon structures associated with the Darrington–Devils Mountain fault zone suggest left-lateral transpression in the
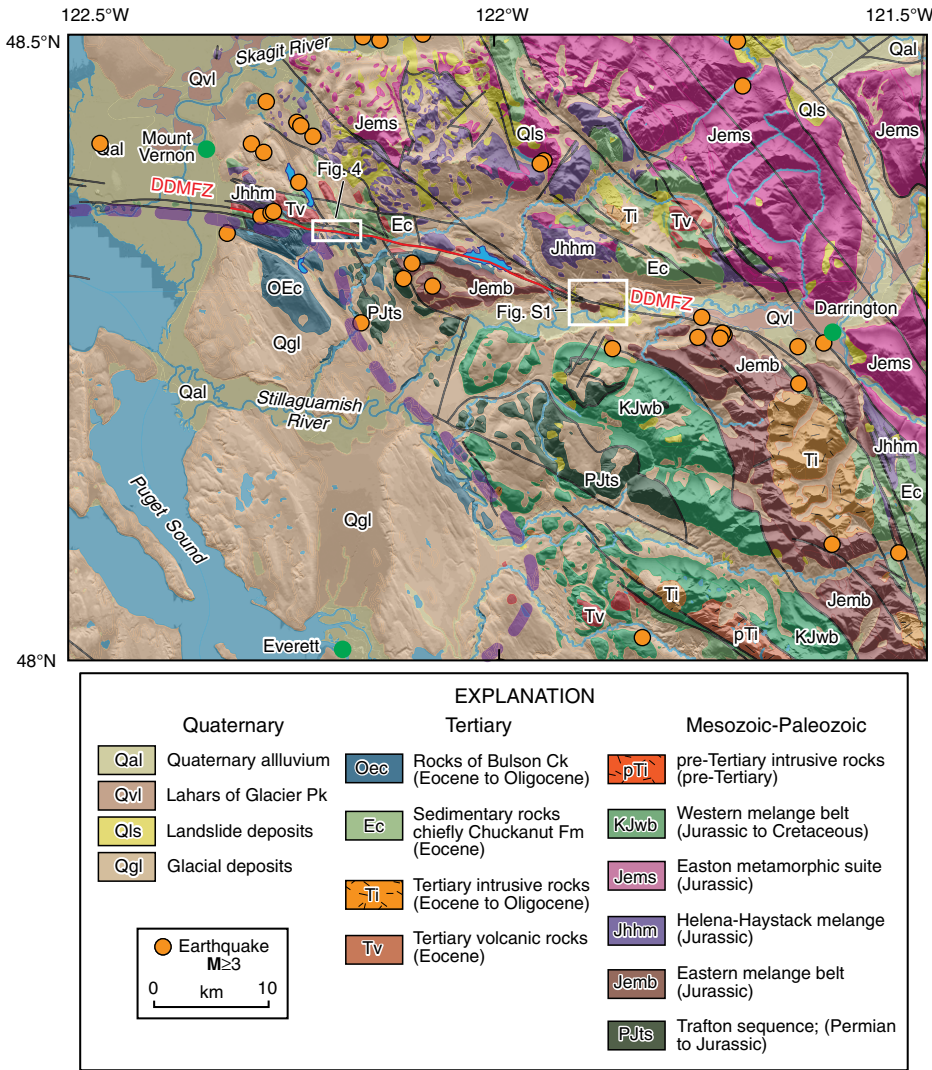
Figure 2. Geologic map of eastern half of Darrington–Devils Mountain fault zone and environs (modified from digital 1:100,000 scale geologic map files from Washington Division of Geology and Earth Resources, 2010). Probable Holocene-active section of Darrington–Devils Mountain fault zone is shown in red; seismicity (orange circles) is from same catalog as Fig. 1B.

later part of its history (Loveseth, 1975; Johnson et al., 2001; Hayward et al., 2006; Dragovich and DeOme, 2006), perhaps due to collision of the Siletzia block in the Eocene (Wells et al., 2014). Historic seismicity is sparse along the mapped trace of the Darrington–Devils Mountain fault zone (Fig. 1B), but a limited number of published focal mechanisms of nearby earthquakes are consistent with the N-S compressive stress regime in the region (Fig. 3).

PREVIOUS INVESTIGATIONS

The first major study of the seismic potential of the Darrington–Devils Mountain fault zone was conducted as part of seismic hazard investigations related to the proposed siting of a nuclear power plant in the Skagit River valley east of Mount Vernon, Washington (Puget Sound Power and Light, 1974; hereafter "Puget Power, 1974"). Puget Power used geologic, air photo, and side-looking airborne radar mapping to locate potentially active fault traces and excavated a total of 11 trenches and eight drill holes at four sites to determine the age of the most recent movement along the fault zone. Puget Power concluded that the Darrington–Devils Mountain fault zone had not been active in the last 35 k.y. and thus was not a capable seismic source (Puget Power, 1974; Bechtel, Inc., 1979; Crosby et al., 1986; Adair et al., 1989).

Extensive studies on Whidbey Island and surrounding marine waters provide abundant evidence of Quaternary deformation along the western portion of the Darrington–Devils Mountain fault zone (Johnson et al., 1996, 2001; Hayward et al., 2006). Johnson et al. (1996, 2001) used water well data, shoreline bluff exposures, and high-resolution seismic profiles to document displacements in last interglacial (oxygen isotope stage [OIS] 5, 80–125 ka) and younger deposits. Although the Darrington–Devils Mountain fault zone has no topographic expression where it projects across Whidbey Island, Johnson et al. (2001) described warping and minor offsets of postglacial (latest Pleistocene to Holocene) sediments in several marine seismic profiles west of Whidbey Island. In subsequent mapping in the area, Dragovich et al. (2005) delineated several strands of the Darrington–Devils Mountain fault zone across the island and inferred that deposits of the latest Pleistocene final glacial recession (Everson interstade) were offset by the Darrington–Devils Mountain fault zone in several cross sections. Hayward et al. (2006) reinterpreted the same seismic data used by Johnson et al. and concluded that the youngest deformation in the eastern Strait of Juan de Fuca makes a right step from their "primary" fault strand of the Devils Mountain fault onto the nearby Utsalady fault. Johnson et al. (2004) conducted a paleoseismic (trenching) investigation of the Utsalady fault and found evidence of multiple Holocene left-lateral transpressional earthquake ruptures. However, no such investigations of the timing of paleoearthquakes have been conducted on the main trace of the Darrington–Devils Mountain fault zone.

Folding and faulting of latest Pleistocene and Holocene lake sediments beneath Lake Cavanaugh (Fig. 3) imaged in high-resolution seismic profiles (Naugler et al., 1996) extend evidence of Quaternary displacement on the Darrington–Devils Mountain fault zone 40–50 km east of Whidbey Island. Although the seismic data are unpublished, Naugler et al. (1996) described a central graben with vertical offset of lake bottom sediments of 3–5 m and used deformation patterns in postglacial sediments to infer a predominant strike-slip component. In later mapping, Dragovich et al. (2004) inferred a similar amount of latest Quaternary vertical offset across their "main strand" of the Darrington–Devils Mountain fault zone under Lake Cavanaugh.

Recent 1:24,000 scale quadrangle geologic mapping, from Whidbey Island on the west to near Darrington on the east, documented abundant evidence of Quaternary displacement along the Darrington–Devils Mountain fault
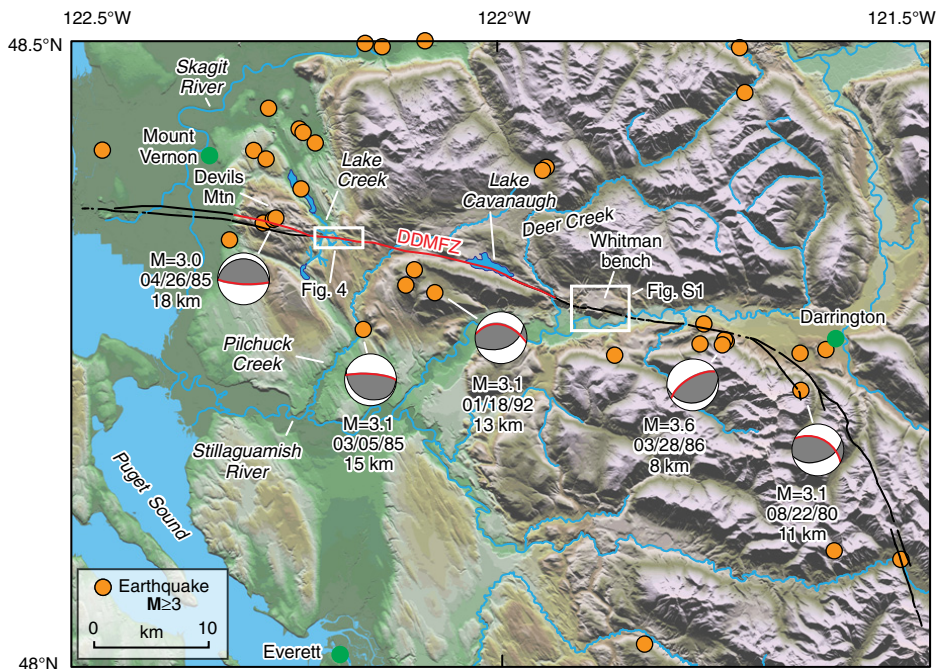
Figure 3. Seismicity (orange circles) of eastern part of Darrington–Devils Mountain fault zone (same catalog as Fig. 1B). Red lines in focal mechanisms are our preferred fault planes. Focal mechanism sources: 04/26/1985—Ma et al. (1996); 03/05/1985, 01/18/1992, and 08/22/1980—Van Wagoner et al. (2002); 03/28/1986—Zollweg and Johnson (1989).

zone (see summary in Dragovich and DeOme, 2006). Such evidence includes possible uplifted alluvial deposits, apparent thinning of valley-fill sediments across the fault zone, observations of sheared Pleistocene sediments, and an anomalous increase in the gradient of Pilchuck Creek (Fig. 3) upstream of the mapped main trace of the Darrington–Devils Mountain fault zone. Dragovich and DeOme (2006) also reinterpreted the trenching study of Puget Power (1974) and concluded that the offset features mapped in some of the Puget Power trenches as slump scarps were instead likely caused by Holocene tectonic movement along the Darrington–Devils Mountain fault zone.

RESULTS OF CURRENT INVESTIGATION

Trenching Investigations

We began our study of the Darrington–Devils Mountain fault zone with a trench investigation on a remnant of glacial outwash (herein informally named the Whitman bench after nearby Whitman Road) perched ~200 m above and north of the modern floodplain of the North Fork Stillaguamish River ~20 km west of Darrington, Washington (Fig. 3). Dragovich et al. (2003a, 2003b) mapped the abandoned

outwash plain as recessional outwash of the Everson interstade of the Fraser glaciation. We excavated two trenches across a 0.75-km-long NW-trending scarp that was first identified by Ralph Haugerud of the U.S. Geological Survey (USGS) on digital elevation models (DEMs) derived from a detailed LiDAR survey of the region (R.A. Haugerud, 2007, written commun.). We found no evidence of tectonic faulting or folding in either trench, and we conclude that the trenched scarp is a glacial-fluvial channel margin rather than a fault scarp. Large-scale logs, unit descriptions, a detailed geomorphic map, and a brief summary of the results of this investigation are included in Supplemental Figure S1[1].

The second phase of our investigation consisted of a trenching study of topographic lineaments in the Lake Creek area (Fig. 4) that were originally identified during the Puget Power (1974) investigation of the Darrington–Devils Mountain fault zone. Our evaluation of the Puget

Power study in the Lake Creek area (see Supplemental Fig. S2[2]) reached conclusions similar to those of Dragovich and DeOme (2006): The lineaments identified by Puget Power are fault scarps marking the trace of the Darrington–Devils Mountain fault zone rather than slump headscarps as originally interpreted by Puget Power. We used the subsurface investigations of Puget Power (1974), detailed geologic mapping of Dragovich and DeOme (2006), and our own field and LiDAR investigations to site our trenches in the Lake Creek area. Our mapping of fault scarps on 2006 LiDAR DEMs (pixel size 1.8 m) resulted in a pattern of late Quaternary faulting in the area (Fig. 4A) similar to that of Dragovich and DeOme (2006). We both map a pair of E-W–trending fault scarps, an ~1-km-long, south-facing northern strand, and an ~0.5-km-long, predominantly north-facing southern strand (graben faults B and A, respectively, of Dragovich and DeOme, 2006). The major difference is that we were unable to confirm the existence of Dragovich and DeOme's (2006) "main strand" that they mapped cutting Vashon-aged glacial deposits 20–50 m north of our northern strand. We found no topographic expression of their main strand either in the LiDAR data or in limited field searches, and none is shown in cross-section B–B′ of Dragovich and DeOme (2006). Puget Power (1974) also showed no indication of faulting, such as offset or truncated bedding or fracturing of the glacial sequence or sheared bedrock within 30–40 m of the projected location of this strand in their log of trench 1A (Supplemental Fig. S2 [see footnote 2]), which extended across the mapped trace of Dragovich and DeOme's (2006) main strand. These lines of evidence and the fact that most of the evidence for significant Quaternary displacement is restricted to the northern strand, support our contention that the northern strand is the surface expression of the steeply dipping active trace of the Darrington–Devils Mountain fault zone.

We excavated three trenches on the northernmost scarp at the Lake Creek site (Fig. 4B) for the following reasons: (1) the northern scarp is longer and more continuously expressed in the landscape than the southern scarp; (2) the Puget Power trenches and drill holes across the northern scarp show significant (as much as 10 m or

---

[1]Supplemental Figure S1. Location map, large-scale logs, photo mosaics, unit descriptions, and summary of results of Black Slug and Horsefly trenches on the Whitman bench. If you are viewing the PDF of this paper or reading it offline, please visit http://dx.doi.org/10.1130/GES01067.S1 or the full-text article on www.gsapubs.org to view Supplemental Figure S1.

[2]Supplemental Figure S2. Scans and authors' reinterpretations (red text) of selected parts of four original logs of excavations (trenches 1A, 1B, 1D, and 1E) and one cross section of drill-hole data from investigations of trench site 1 of Puget Power (1974). Reproduced with permission of Puget Sound Energy, 11/21/2013. If you are viewing the PDF of this paper or reading it offline, please visit http://dx.doi.org/10.1130/GES01067.S2 or the full-text article on www.gsapubs.org to view Supplemental Figure S2.
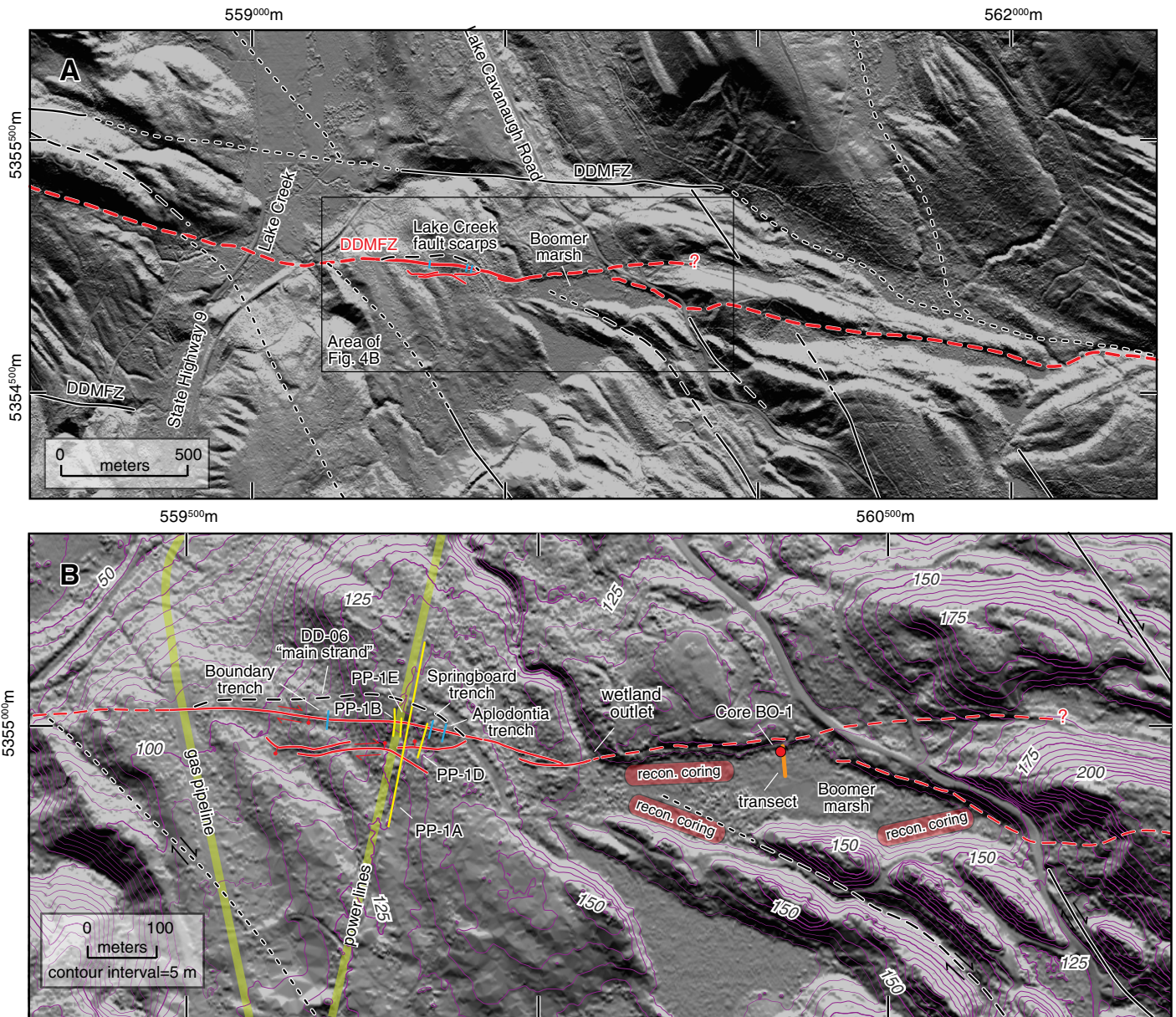
Figure 4. Map of Darrington–Devils Mountain fault zone (DDMFZ) in vicinity of Lake Creek (see Figs. 2 or 3 for figure location). (A) Overview map showing Holocene-active (red lines) and other traces (black lines) of Darrington–Devils Mountain fault zone and ancillary faults, modified from Dragovich and DeOme (2006). Long-dashed faults are inferred; short-dashed faults are concealed. (B) Enlarged map showing locations of three trenches from current study (heavy blue lines), and approximate locations of four trenches from previous investigations (yellow lines) related to proposed Skagit Nuclear Power Project (Puget Power, 1974). Also shown are locations of core BO-1 (red circle), detailed coring transect (heavy orange line) and areas of reconnaissance coring in Boomer marsh. Solid red lines mark the locations of fault scarps along the trace of Darrington–Devils Mountain fault zone as mapped on light detection and ranging (LiDAR) digital elevation models (DEMs) in the current study; dashed red lines where inferred. Long-dashed black line just north of our trenches is left-lateral, south-side-up oblique "main strand" as mapped by Dragovich and DeOme (2006). NW-striking black lines are right-lateral bedrock faults thought to be subsidiary to Darrington–Devils Mountain fault zone (Dragovich and DeOme, 2006). Base map is hillshaded DEM derived from LiDAR data (pixel size 1.8 m) from Puget Sound LiDAR Consortium; illumination from azimuth 05°, at 5° above the horizon; datum is NAD83, UTM zone 10N.

more) north-side-up vertical separation of the bedrock surface (Supplemental Fig. S2 [see footnote 2]), consistent with the sense of slip inferred along the northern scarp; and (3) vertical separation of the bedrock surface is much smaller (<4 m) and evidence of faulting is more ambiguous where Puget Power (1974) trenches 1A and 1D cross the southern scarp (Supplemental Fig. S2 [see footnote 2]). We consider the southern scarp as a minor splay of the main (northern) strand that likely has a similar history of Quaternary faulting.

We excavated the easternmost "Aplodontia" and "Springboard" trenches ~25 m apart across an ~1-m-high south-facing scarp (Fig. 5;
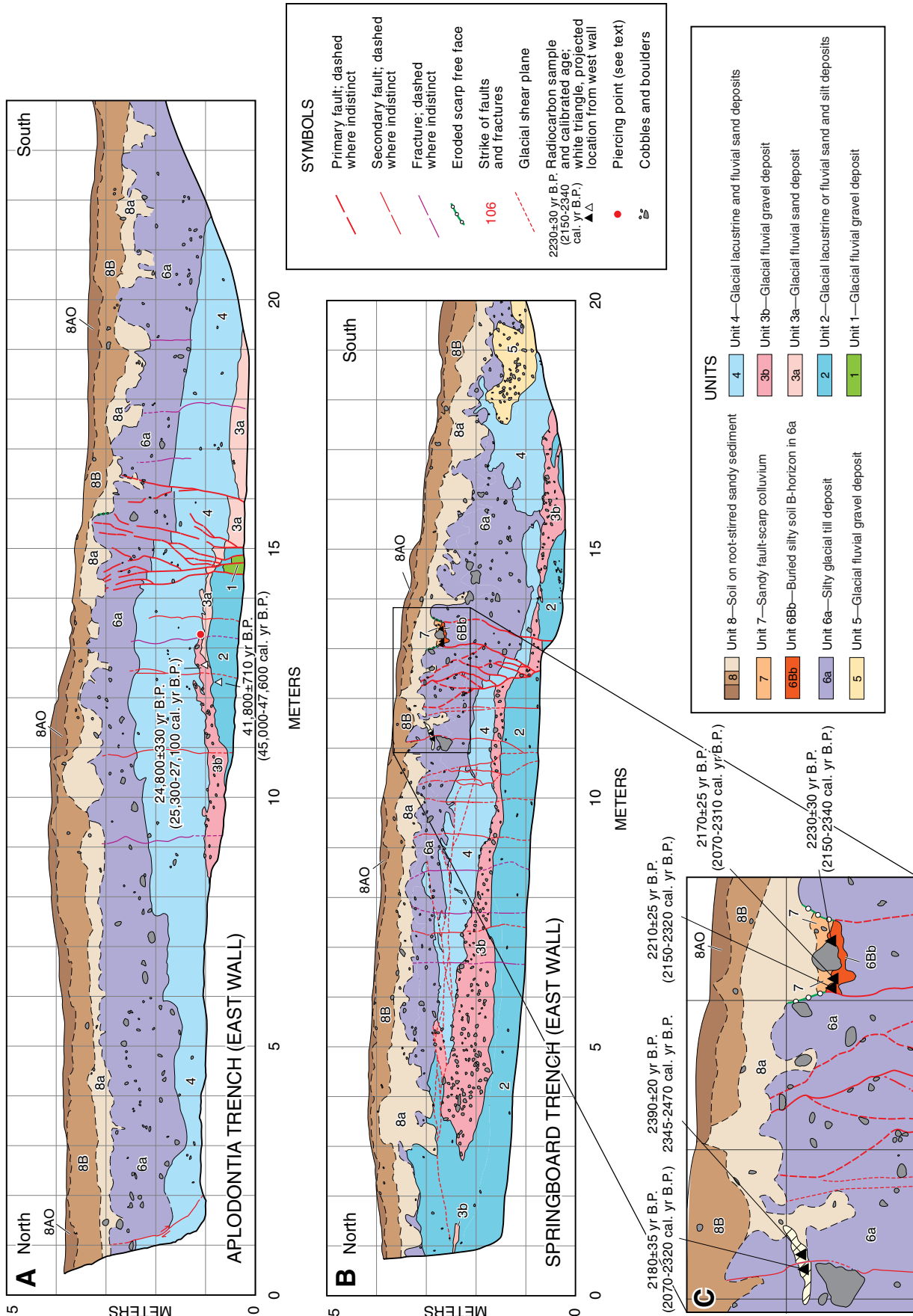
Figure 5. Simplified logs of (A) Aplodontia and (B) Springboard trenches across Darrington–Devils Mountain fault zone at Lake Creek site; (C) enlarged area of fault zone, buried soil (unit 6Bb), and scarp-colluvial deposit (unit 7) in Springboard trench. See Supplemental Figure S3 (see text footnote 3) for larger-scale logs, photo mosaics, and unit descriptions.

Supplemental Fig. S3[3]) and exposed a sequence of glacial sediments consisting of a basal unit of lacustrine or fluvial sand and silt (unit 2), which overlies and is faulted against a fault-bounded remnant of fluvial gravel (unit 1). These basal units are overlain by a 30- to 90-cm-thick deposit of fluvial (outwash) sand and gravel (unit 3). We use the abrupt transition from gravel (unit 3b) to sand (unit 3a) in the Aplodontia trench at horizontal trench m 13.25 as a piercing point in a later analysis of lateral slip across the fault zone (see "Fault Geometry and Sense of Slip"). A massive to moderately bedded lacustrine and fluvial deposit of sand and silty sand (unit 4) overlies unit 3. An up to 2-m-thick deposit (unit 6a) of massive silt and silty sand (till) caps the glacial sequence. An extensively root-stirred soil (unit 8) is formed in the upper part of unit 6. The trenched deposits are mapped as part of the Vashon Stade advance of the Fraser glaciation (Dragovich and DeOme, 2006). Dragovich and DeOme (2006) used a radiocarbon age (14,725 ± 470 radiocarbon yr B.P.; 17.9 ± 1.0 ka [thousands of calibrated years ago, ±2σ]) from a depth of 3 m in Puget Power (1974) trench 1B (70 m west of the Aplodontia trench) to date the glacial sequence at the Lake Creek site. This age is in agreement with the timing of the advance and retreat of the Puget Lobe of the Cordilleran ice sheet during the Fraser glaciation (Porter and Swanson, 1998). Two radiocarbon samples (Table 1) from a depth of 3.2 m in unit 2 (45.3 ± 1.1 ka) and 2.8 m in unit 3b (26.2 ± 1.1 ka) in the Aplodontia trench may indicate a pre-Vashon age for the lower part of the sequence. However, because both of these samples were on detrital charcoal, we consider them to be maximum-limiting ages for the glacial sediments exposed in the Lake Creek trenches.

In both trenches, the glacial sequence is bisected by a near-vertical, 2-m-wide fault zone with 45–70 cm of up-to-the-north vertical separation (Fig. 5; Supplemental Fig. S3 [see footnote 3]). Several near-vertical fractures and faults with millimeter-scale vertical displacements extend 4–6 m north and as much a 4 m south of the main fault zone, but they are more numerous and more continuous north of the fault zone. Many of the faults and fractures continue upward through the glacial sequence but were difficult to map in the root-stirred soil horizons that cap the sequence. Remnants of a charcoal-rich buried soil on the glacial deposits

[3]Supplemental Figure S3. Large-scale logs, photo mosaics, and unit descriptions of Aplodontia, Springboard, and Boundary trenches at the Lake Creek site. If you are viewing the PDF of this paper or reading it offline, please visit http://dx.doi.org/10.1130/GES01067.S3 or the full-text article on www.gsapubs.org to view Supplemental Figure S3.

TABLE 1. RADIOCARBON DATA FROM WHITMAN BENCH AND LAKE CREEK SITES, DARRINGTON–DEVILS MOUNTAIN FAULT ZONE

Sample no.	Lab no.	Unit	Sample weight (mg)	δ13C (‰)	Reported age* (14C yr B.P. ± 1σ)	Calibrated age range (cal. yr B.P. ± 2σ)	Calibrated age† (wt mean ± 2σ)	Comments
Whitman bench, Horsefly trench								
WB-HF-R01	OS-65837	3			5900 ± 35	6800–6640	6720 ± 80	1 angular fragment unidentified charcoal; too young
Lake Creek, Puget Power (1974) trench 1B, depth 3 m								
		2, 3?			14,725 ± 470	18,820–16,920	17,910 ± 1020	Charcoal in outwash sand, 3 m depth
Lake Creek, Springboard trench, east wall								
ARN08-01S	OS-70184	Root cast	29.6	−26.04	2180 ± 35	2330–2060	2210 ± 130	1 angular fragment burned root charcoal
ARN08-02S	OS-71477	Root cast	57.5	−26.25	2390 ± 20	2470–2340	2410 ± 110	1 angular fragment burned root charcoal
ARN08-04S	OS-70185	6Bb	38	−25.81	2230 ± 30	2340–2150	2240 ± 110	1 angular fragment unidentified charcoal, flattened by boulder
SB-R01	OS-71776	6Bb	54.4	−25.96	2210 ± 25	2320–2150	2230 ± 100	1 angular fragment unidentified charcoal, in buried soil or in block of prefault soil in overlying colluvium
SB-R02a	OS-71526	6Bb	27.5	−26.39	2170 ± 25	2310–2060	2210 ± 130	1 angular fragment unidentified charcoal from outer shell of block (log?) of wood charcoal in buried soil
NA	–	–	–	–	–	2310–2150	2230 ± 100	Weighted average of four ages (ARN08-01S, ARN08-04S, SB-R01, SB-R02a); max. age of youngest trench EQ
Lake Creek, Aplodontia trench, west wall								
ARN08-07A	OS-71770	3b	67.8	−25.95	21,800 ± 330	27,510–25,090	26,200 ± 1080	1 fragment unidentified charcoal; max. age
ARN08-08A	OS-71775	2	27.3	−27.51	41,800 ± 710	46,410–44,270	45,310 ± 1110	1 fragment unidentified charcoal; max. age
Lake Creek, Boomer marsh core BO-1								
BO-69-R1	OS-88352	6	2.3	−27.24	1460 ± 25	1390–1300	1350 ± 50	Top of core; flattened leaf fragments
BO-75-R2	OS-88390	6	5.3	−23.71	1600 ± 30	1550–1410	1480 ± 80	Fragments of unidentified terrestrial beetle
BO-77-R3	OS-88353	5	9.5	−25.61	1920 ± 30	1950–1740	1870 ± 70	Angular fragments of unidentified charcoal; 200–300 yr too old, based on bracketing seed and insect ages
BO-78-R11	OS-90897	5	1.4	−25.04	1760 ± 25	1770–1560	1670 ± 80	2 seeds and 1 seed case, unidentified wetland herb
BO-88-R12	OS-90984	4	2.6	−25	Modern	–	–	Sitka spruce needles
BO-89-R4	OS-88354	4	9.7	−25.67	2840 ± 30	3070–2860	2950 ± 100	Angular fragments of unidentified charcoal; 900–1100 yr too old, based on bracketing seed and charcoal ages
BO-97-R5	OS-88355	4	10	−26.39	2320 ± 30	2440–2180	2330 ± 80	Angular fragments of unidentified charcoal
BO-98-R13	OS-90834	4	10.8	−28.08	1610 ± 25	1550–1410	1480 ± 80	Angular fragments of detrital wood
BO-100-R14	OS-91018	3	5.0	−24.34	5010 ± 50	5900–5640	5760 ± 150	Angular fragments of unidentified charcoal
BO-103-R15	OS-90837	3	4.1	−27.15	Modern	–	–	Sitka spruce needles
BO-115-R7	OS-88380	2	5.2	−23.19	6930 ± 50	7930–7670	7770 ± 120	1 seed, *Brasenia schreberi* (watershield)
BO-123-R8	OS-88381	2	11.6	−22.34	7260 ± 35	8170–8000	8090 ± 100	2 seeds, *Brasenia schreberi* (watershield)
BO-124-R16	OS-90840	1	9.2	−23.58	7280 ± 30	8170–8010	8100 ± 90	2 seeds, *Brasenia schreberi* (watershield)
BO-125-R9	OS-88382	1	7.9	−25.73	Modern	–	–	Sitka spruce needles
BO-135-R10	OS-88383	1	24.7	−22.09	8090 ± 40	9240–8780	9020 ± 140	Base of core; 4 seeds, *Brasenia schreberi* (watershield)

*Ages in bold were used to calculate weighted average estimate (2230 ± 100 cal. yr B.P.) of maximum age of youngest earthquake observed in Springboard trench (see Fig. 11B).
†Ages in bold were used in OxCal model (Fig. 11B).

(unit 6Bb) and an overlying 10- to 15-cm-thick deposit of fault-scarp colluvium are preserved at the upward terminations of two fault splays in the Springboard trench. In addition, a cast of a large burned root offset by a single fault splay is preserved at a similar stratigraphic level in the upper part of the glacial sequence. Five radio-carbon ages on charcoal from the buried soil and burned root yield similar ages of 2.2–2.4 ka. We also observed a zone of subhorizontal shears and flame-like injections of glacial units 3, 4, and 6 north of the main fault zone in the Spring-board trench. Their strata-bound and rootless geometry leads us to attribute these features to internal glacial deformation, rather than tectonic processes.

We excavated a third ("Boundary") trench ~125 m west of the Springboard trench across a 1.5-m-high scarp on the northern strand to examine along-strike variations in faulting and preservation of near-surface faulting relations. The trench exposed highly sheared bedrock eroded into and overlain by a sequence of gla-cial-fluvial, glacial-lacustrine, and till sediments deposited at the basal glacier-bedrock contact

(Fig. 6; Supplemental Fig. S3 [see footnote 3]). We suspect that the differences in depth to bed-rock between the Aplodontia/Springboard and Boundary trenches reflect hydraulic or topo-graphic irregularities in the bed of the overrid-ing ice sheet, rather than differences in vertical displacement between the two sites. The base of the glacial sequence consists of gravelly till (unit 3) and glacial-lacustrine sand and silt (unit 4) deposits locally preserved in subglacial chan-nels or tunnels eroded into the underlying bed-rock. The surficial and bedrock deposits were subsequently planed off by later glacial erosion. The unconformity created by this erosion event is marked throughout most of the trench by a thin (5–10 cm) deposit of lacustrine or fluvial silt to fine sand. This marker bed is in turn over-lain by glacio-fluvial and till deposits (unit 6) of gravelly silt and sand. The sequence is capped by a gravelly glacio-fluvial deposit (unit 7) and a thick root-stirred soil (unit 8) formed in unit 7. Bedrock exposed in the bottom of the trench includes highly weathered sandstone and shale (unit 1) north of the fault zone, and pervasively sheared and convolutedly bedded

sandstone, shale, and coal (unit 2) to the south. As mapped in the immediate area, these rocks probably correspond to the Eocene Chuckanut Formation and Oligocene to Eocene Rocks of Bulson Creek, respectively (Dragovich and DeOme, 2006).

The Boundary trench exposed a complex, steeply dipping, 1- to 1.5-m-wide zone consist-ing of two primary synthetic faults similar to those exposed in the Aplodontia and Spring-board trenches. The numerous strands that com-prise the fault zone continue upward through the glacial sequence until they are obscured by soil formation in unit 8. The thin marker bed at the bedrock-glacial contact (unit 5) is verti-cally separated 65 cm (up-to-the-north) across the fault zone. Abrupt changes in geometry and thickness of units 4 and 6 are apparent across the fault zone. Abundant evidence of pregla-cial deformation in the bedrock units includes two shear zones in the steeply dipping, highly weathered sandstone and shale in the footwall, and pervasive shearing and convoluted bedding in unit 2 in the 15-m-wide exposure of these rocks in the hanging wall. The coincidence of
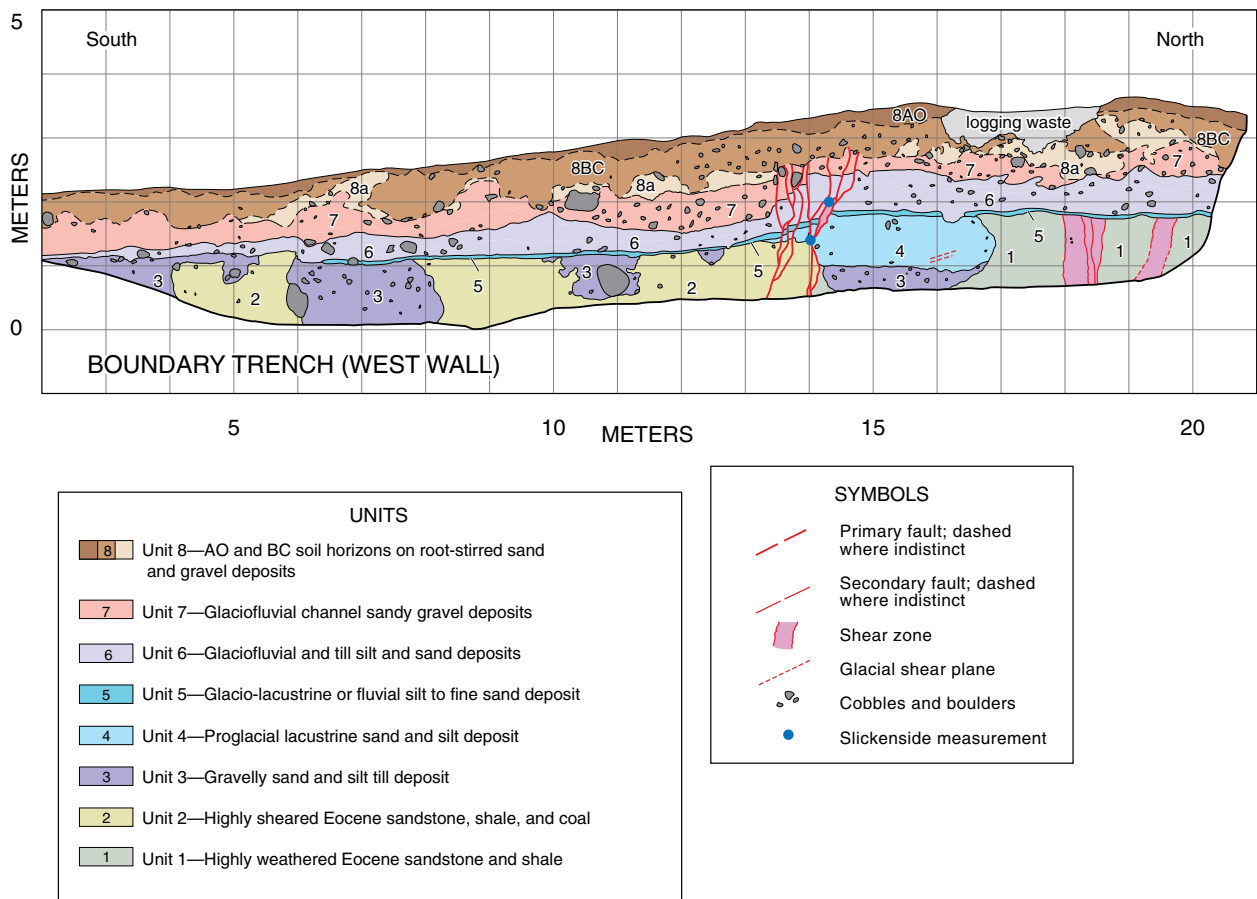

Figure 6. Simplified log of Boundary trench across Darrington–Devils Mountain fault zone at Lake Creek site. See Supple-mental Figure S3 (see text footnote 3) for larger-scale log, photo mosaic, and unit descriptions.

Quaternary faulting with such an abrupt change in bedrock properties is evidence that this strand of the Darrington–Devils Mountain fault zone has likely been recurrently active for millions of years.

We documented two sets of slickensides on the two primary postglacial fault traces in the Boundary trench. In the east wall, two slickenlines in highly sheared bedrock (unit 2) plunge 40° and 58° west on the western primary fault strand (Fig. 7), and in the west wall, two slickenlines in fine-grained glacial sediments (units 4 and 6) plunge 02° and 07° east on the eastern primary fault strand. The implications of these features are discussed in the "Fault Geometry and Sense of Slip" section later herein.

After opening the Lake Creek trenches, we recognized the probability of significant strike-slip displacement based on the very steep fault dips, flowerlike fault geometries, slickenside orientations, and major changes in the thickness and texture stratigraphic units across faults. To further explore the question of slip direction, we dug additional excavations adjacent to the Aplodontia and Boundary trenches near the end of our field investigation to quantify the sense and amount of postglacial lateral slip. The logs from these excavations are shown in Supplemental Figures S4[4] and S5[5], and the implications of these results are discussed in detail in Figures 8 and 9 and the "Fault Geometry and Sense of Slip" section.

Results of Boomer Marsh Investigation

The third phase of our investigation focused on refining the earthquake chronology on the Darrington–Devils Mountain fault zone. The three trench exposures at the Lake Creek site showed an almost complete lack of preservation of fault-related stratigraphy (e.g., scarp-derived colluvium) in the upper 0.5–1 m due to soil formation and extensive churning of the glacial sequence by root growth, tree-throw cratering, and burrowing animals. We only found evidence of a single earthquake-related deposit in one trench (scarp-colluvial unit 7 in Springboard trench; Fig. 5; Supplemental Fig. S3 [see footnote 3]), despite the presence in all three

---

[4]Supplemental Figure S4. Map and logs of slot trenches indicating right-lateral slip in the vicinity of the Aplodontia trench. If you are viewing the PDF of this paper or reading it offline, please visit http://dx .doi.org/10.1130/GES01067.S4 or the full-text article on www.gsapubs.org to view Supplemental Figure S4.

[5]Supplemental Figure S5. Map and logs of slot trench indicating right-lateral slip in the vicinity of the Boundary trench. If you are viewing the PDF of this paper or reading it offline, please visit http://dx .doi.org/10.1130/GES01067.S5 or the full-text article on www.gsapubs.org to view Supplemental Figure S5.
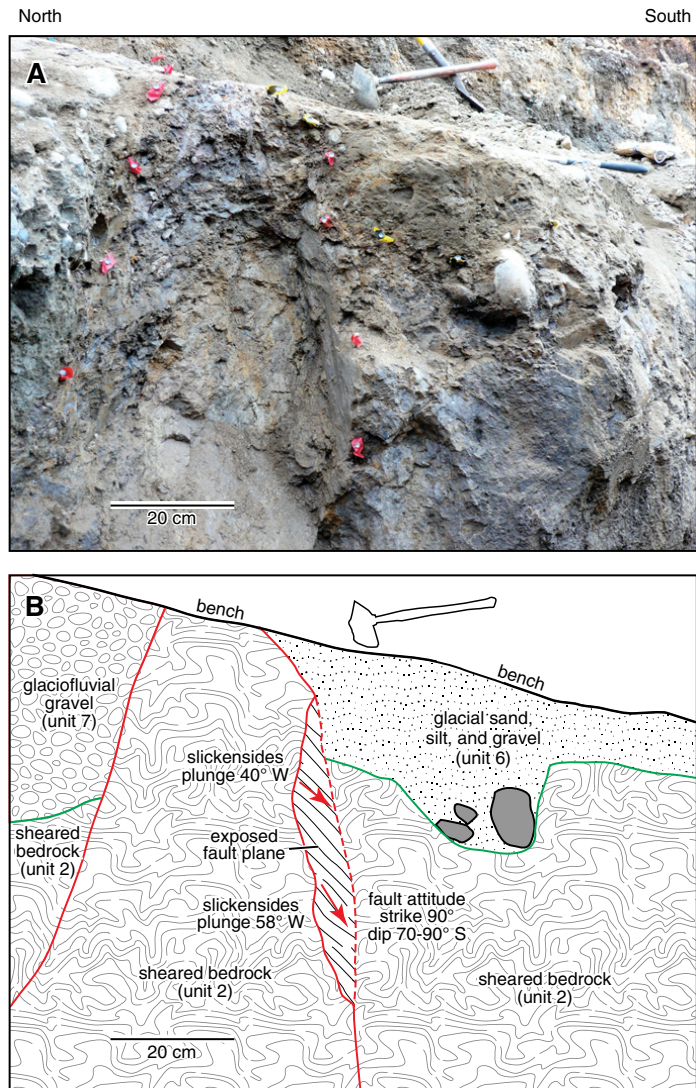

Figure 7. Photograph (A) and line drawing (B) of slickensides in bedrock on one of the primary traces of the Darrington–Devils Mountain fault zone exposed in east wall of Boundary trench; see Figure 6 and Supplemental Figure S3 (see text footnote 3) for unit descriptions. Direction of plunge indicates right-lateral oblique sense of slip.

trenches of numerous fault splays that likely ruptured the ground surface. In order to help refine the age of this earthquake and to look for evidence of other earthquakes that may have been obscured by soil formation, we conducted a coring investigation of a small wetland (herein informally referred to as "Boomer marsh") directly adjacent to the eastern end of the Lake Creek fault scarps (Fig. 4A).

In our refinement of Dragovich and DeOme's (2006) mapping of the Lake Creek fault scarps, we mapped the eastern end of the northern LiDAR scarp to within a few tens of meters of the outlet of Boomer marsh (Fig. 4B). Drago-

vich and DeOme (2006) mapped the fault to the southeast as concealed beneath the center of the marsh, but the similar trend of the steep scarp that forms the northern margin of the marsh suggested to us that the Lake Creek fault scarp might instead project across the outlet of the Boomer marsh and continue eastward along the northern margin. If our mapping is correct, then a record of scarp formation during earthquakes might be manifested in the marsh stratigraphy by: (1) temporary deepening of the marsh by partial damming of the outlet, and (2) incursion of slope colluvium onto the near-shore marsh surface from exposure of glacial
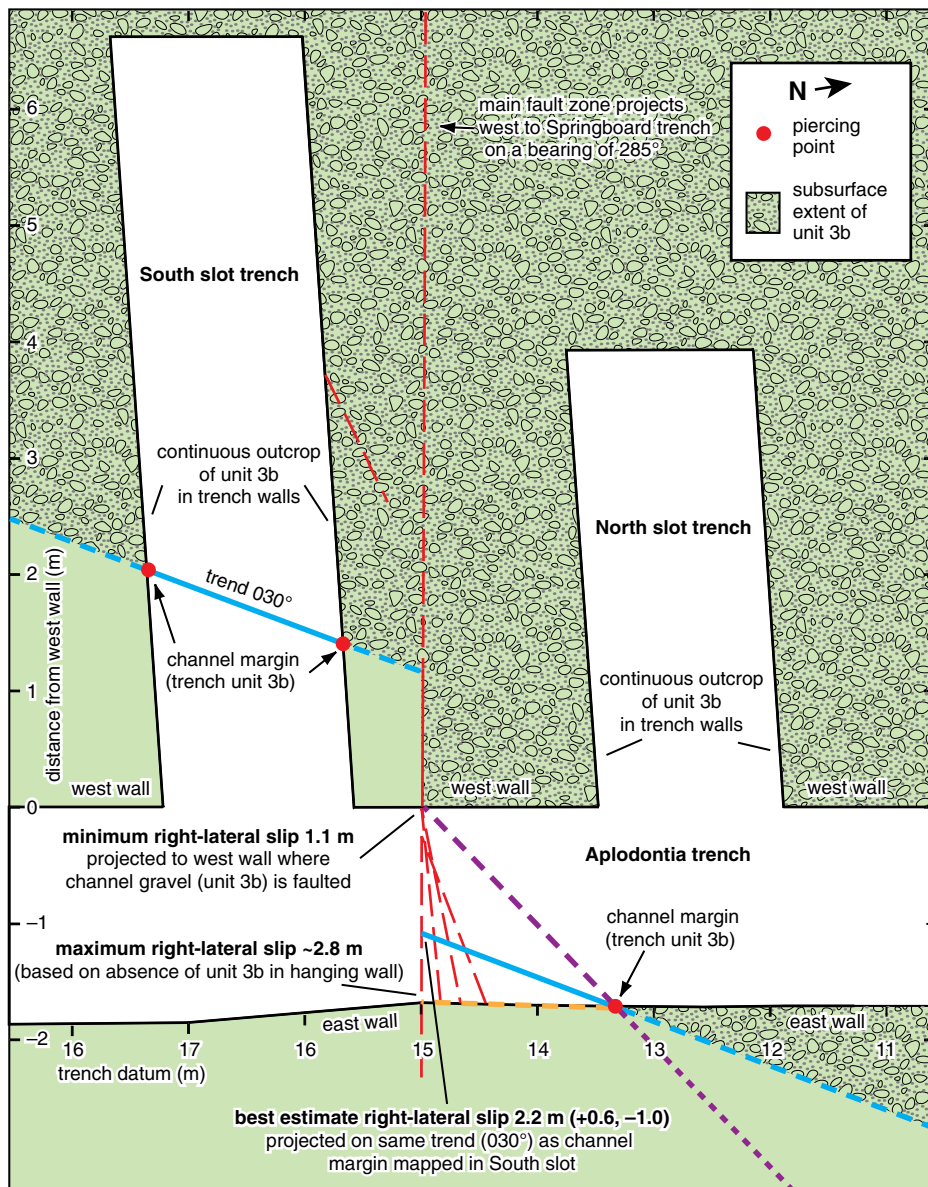
Figure 8. Planimetric map and measurement of apparent right-lateral offset of channel margin of glacial-fluvial unit 3b in Aplodontia slot trenches. Projection lines illustrate three estimates of right-lateral offset: blue lines show our best estimate, projected on same trend as channel margin in south slot trench; purple and orange lines illustrate estimates of minimum and maximum right-lateral slip, respectively. Note the numerous fault traces in the east wall (Fig. 5A) that coalesce into a simple single trace at the base of the west wall. See Supplemental Figure S4 (see text footnote 4) for detailed logs of slot trench walls.

sediments by surface faulting along the northern margin of the marsh.

Our initial series of exploratory 1- to 6-m-deep gouge cores along the northern edge of the marsh revealed a laterally extensive stratigraphic sequence consisting of a basin-ward-thinning package of sandy and pebbly silts, over- and underlain by thick peat deposits. In contrast, reconnaissance coring along the southern edge of the marsh, which is marked by

higher, steeper slopes in thin glacial deposits and sandstone bedrock (Dragovich and DeOme, 2006), revealed highly variable sequences of peat, lacustrine silt, and rocky debris; we infer the latter sediments were deposited by localized slope failures. We found no evidence of a basinward-thinning silty sequence similar to the northern margin in exploratory cores at numerous sites distributed along the southern margin (Fig. 4B).

We documented the geometry of the silty sequence present along the northern margin with six, 2.5-cm-wide gouge cores along a 40-m-long transect from the wetland edge to near the center of the marsh (Fig. 4B). We determined the gross stratigraphy with small gouge cores (Fig. 10; Supplemental Fig. S6[6]), and then we used a "Russian" coring device to obtain a larger-diameter (5-cm-wide), 70-cm-long core of the middle part of gouge core BO-01 for sedimentologic analysis and sampling (Fig. 11A; Supplemental Fig. S7[7]). In the laboratory, we made detailed sediment descriptions using the methods of Troels-Smith (1955), sampled and described diatom assemblages (Supplemental Fig. S8[8]), and carefully sampled for macroscopic samples of plant fragments and charcoal for radiocarbon dating (Table 1; Fig. 11A; Supplemental Fig. S7 [see footnote 7]).

The gouge and Russian cores revealed a sequence of well-bedded silts interbedded with sandy, pebbly silts, over- and underlain by 70- to >100-cm-thick peat deposits. The base of the Russian core consists of 15 cm of sandy decomposed peat, which is overlain in sharp contact by an 11-cm-thick sandy silt interval marked by a 2-cm-thick pebbly sand at its base, which in turn is overlain by a 1-cm-thick bed of mixed organic materials (Fig. 11A; Supplemental Fig. S7 [see footnote 7]). The organic bed grades upward to finely laminated sandy silt and a diatom assemblage indicative of deeper, quiet-water deposition. A peaty interval overlying the sandy silt suggests a temporary shallowing of water depths, but this interval transitions gradually back to deeper water depths with the deposition of ~13 cm of finely laminated silt. The silt interval contains a prominent 2- to

---

[6]Supplemental Figure S6. Field descriptions of small-diameter (2.5 cm) gouge cores in transect across northern part of Boomer marsh. If you are viewing the PDF of this paper or reading it offline, please visit http://dx.doi.org/10.1130/GES01067.S6 or the full-text article on www.gsapubs.org to view Supplemental Figure S6.

[7]Supplemental Figure S7. Photomosaic and unit descriptions (using nomenclature of Troels-Smith, 1955) of colluvial sequence (depth 65–140 cm) in middle part of core BO-1 sampled with "Russian" medium-diameter (5 cm) corer. White dots mark locations of smear slide samples. If you are viewing the PDF of this paper or reading it offline, please visit http://dx.doi.org/10.1130/GES01067.S7 or the full-text article on www.gsapubs.org to view Supplemental Figure S7.

[8]Supplemental Figure S8. Photographs and descriptions of smear slides from colluvial sequence (depth 65–140 cm) in middle part of core BO-1 sampled with "Russian" medium-diameter (5 cm) corer. If you are viewing the PDF of this paper or reading it offline, please visit http://dx.doi.org/10.1130/GES01067.S8 or the full-text article on www.gsapubs.org to view Supplemental Figure S8.
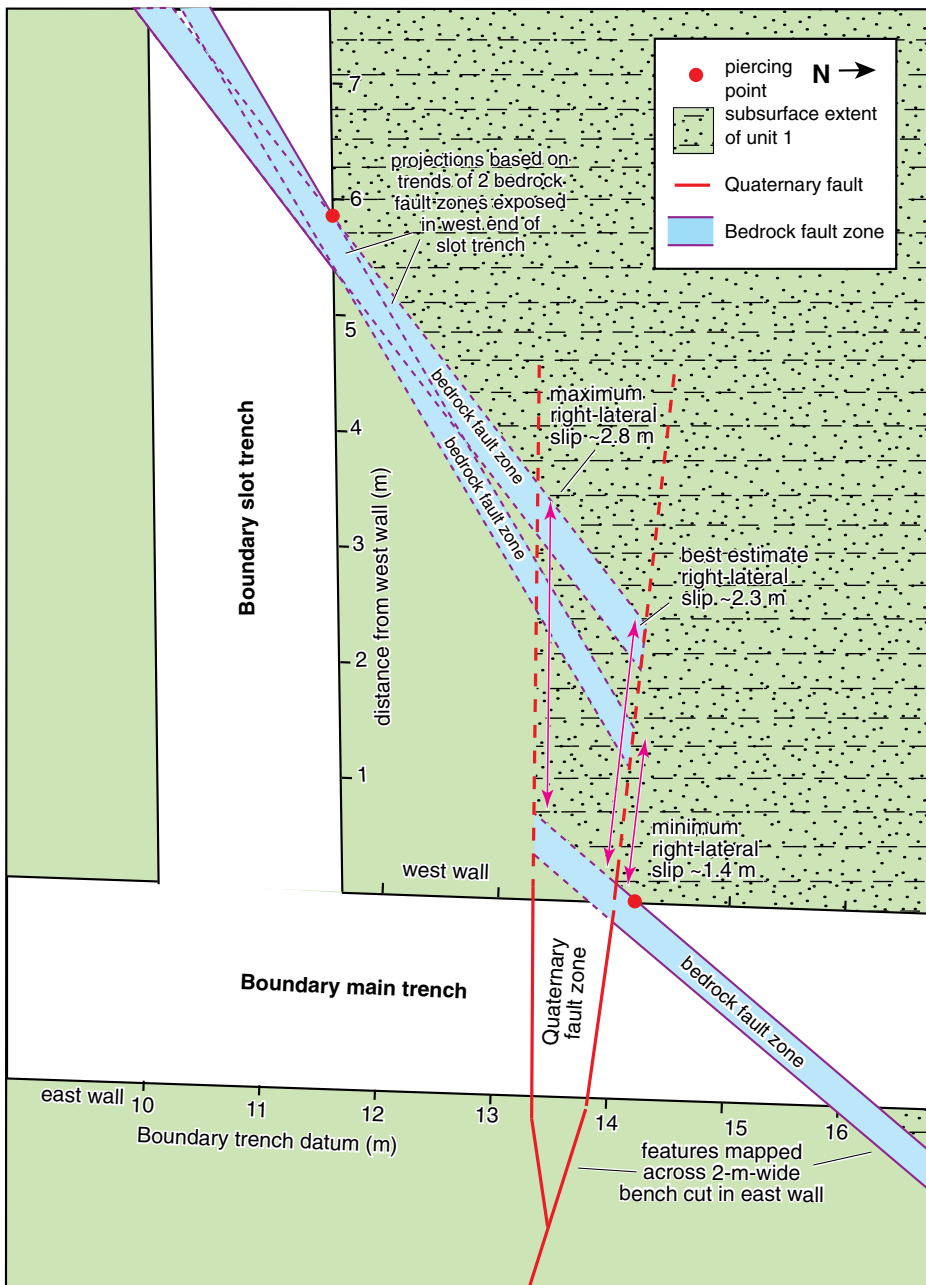
Figure 9. Planimetric map and measurement (with sources of uncertainties) of apparent right-lateral offset of distinctive bedrock fault zone in Boundary slot trench. See Supplemental Figure S5 (see text footnote 5) for detailed logs of slot trench walls.

detrital wood, charcoal, and pebbles. Diatom assemblages suggest somewhat shallower water depths than the lower sandy silt (Fig. 11A). Subsequent deposition of a 5-cm-thick interval of diatomite- and organic-rich silt suggests water depths gradually deepened and then gradually shallowed with a return to peat deposition that extends to the modern-day surface of the marsh.

Interpretation of Boomer Marsh Stratigraphy

The marsh deposits described from the BO-1 core contain two sandy, pebbly silt intervals that we interpret as the sedimentologic response to two periods (colluvial events "CE1" and "CE2") of colluvial progradation of hillslope sediment and organic debris into the marsh. We base this interpretation on the following evidence: (1) Both intervals are wedge-shaped and thin and become finer grained away from the wetland margin. (2) The sharp lower boundaries of both intervals suggest abrupt progradation of hillslope sediment and organic debris into the marsh rather than soil formation on an exposed wetland surface. (3) The presence of sand and pebbles in the basal sediments of both intervals indicates that they likely were derived from exposure of the glacial sediments currently covered by heavy vegetation and thick forest duff in the hillslopes adjacent to the marsh; the lack of any similar deposits in similar geomorphic positions in the rest of our transect or reconnaissance cores likely precludes a fluvial or flood origin for these coarse sediments.

We examined a number of possible origins for the sediments we interpret as colluvium along the northern margin of the Boomer marsh (see "Alternative Explanations" section) before concluding that these deposits were likely the result of one and possibly two surface-rupturing earthquakes on the Darrington–Devils Mountain fault zone. Evidence supporting this conclusion is circumstantial and stronger for CE1 than CE2: (1) Two laterally persistent stratigraphic packages of colluvial deposits are only found adjacent to the steep south-facing scarp that controls the northern margin of the marsh. The approximately E-W trend of the northern margin is parallel to the strike of the LiDAR-defined Lake Creek fault scarps and is anomalous because most nearby steep slopes have NW to WNW strikes controlled by the underlying bedrock (Dragovich and DeOme, 2006). The similar trend and near continuity with mapped fault scarps across the 25-m-wide outlet indicate to us that the surface trace of the Darrington–Devils Mountain fault zone is coincident with the steep slope bordering the northern margin of the marsh (Fig. 4B). This slope has been modi-

3-cm-thick orange tephra bed chemically correlated with the Mazama ash, dated elsewhere (Zdanowicz et al., 1999) at 7630 ± 150 cal. yr B.P. (Supplemental Table S1[9]). The same dis-
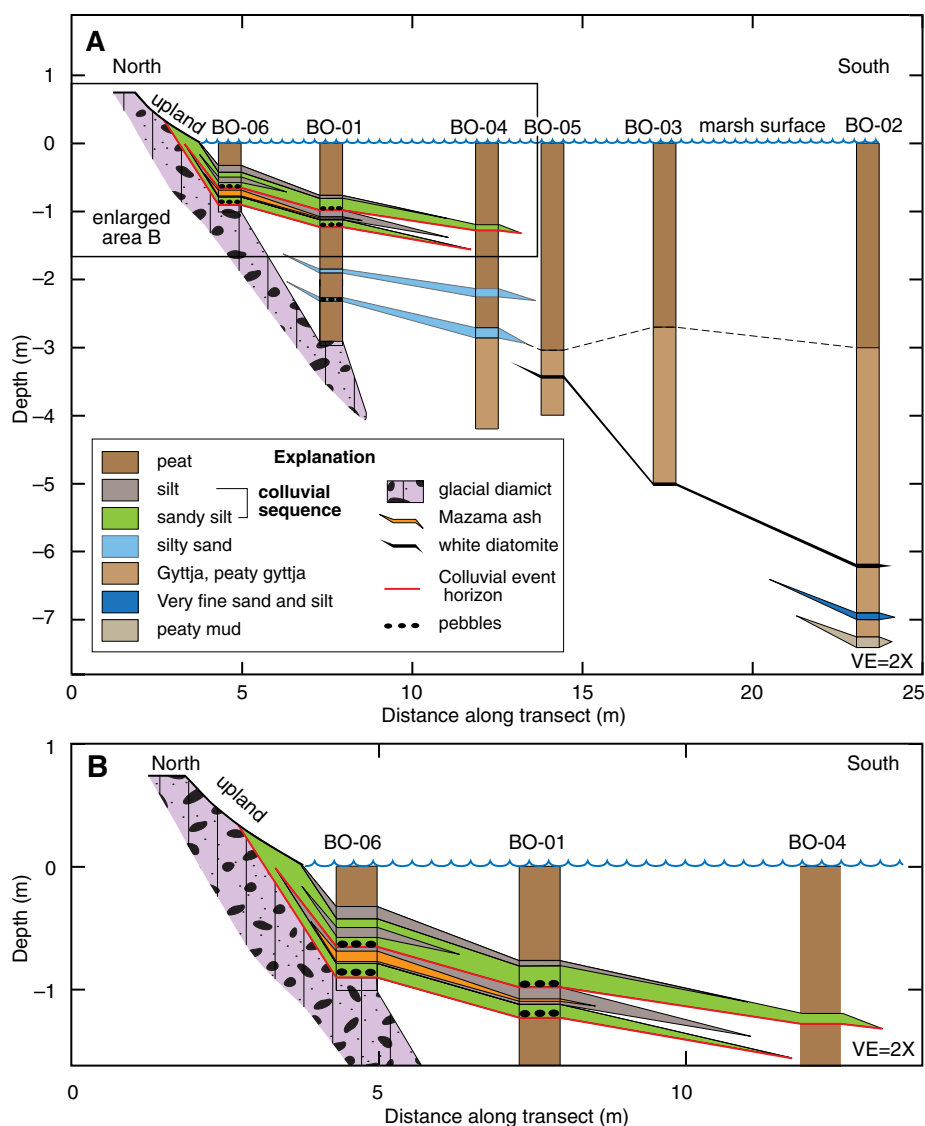
tinctively colored bed was identified in several reconnaissance cores along the northern margin of the marsh west of our transect (Fig. 4B). At a depth of 99 cm, the silt interval is overlain in sharp contact by another sandy silt deposit with a 2-cm-thick basal layer of mixed sand, pebbles, and detrital wood similar to the lower sandy-silt deposit. Above the mixed basal layer, the upper sandy silt interval is discontinuously laminated, but it also contains numerous fragments of

Figure 10. Gouge-core transect across northern part of Boomer marsh; results show two basinward-thinning sequences we interpret as colluvial evidence of two earthquake surface ruptures along the northern margin of the marsh. Two other silty sand deposits were intercepted in the lower parts of cores BO-1 and BO-04. We considered the possibility that these deposits also represented colluvial deposition related to older earthquakes, but we discounted this scenario because both deposits thin toward the margin of the marsh and thus were probably not deposited as wedges of sediment derived from the adjacent hillside. We favor a fluvial origin for these older deposits. See Supplemental Figures S6 and S7 (see text footnotes 6 and 7) for detailed core descriptions. VE—vertical exaggeration.

may have been caused by partial damming of the outlet by formation of a north-side-up fault scarp. Significant deepening apparently did not accompany CE1, either because the earthquake was predominantly strike slip, or because of folding of the northern margin of the marsh. The former is supported by the set of near-horizontal slickensides observed in the Boundary trench, and the latter is supported by the unconformity defined by abrupt changes in sedimentation rates between deposition of the Mazama ash and the time of CE1. We infer that the dearth of evidence for CE2 in our Lake Creek trenches is attributable to near-complete disruption by burrowing animals and root stirring of the upper parts of the glacial deposits exposed in the walls of all three trenches.

Alternative Explanations

We acknowledge that our interpretation of the stratigraphy observed in the Boomer marsh is not unique. Other processes that could produce some of the characteristics we observed in our core transect include (1) water-level fluctuations related to outlet damming by mass wasting or animal activity (beavers), (2), erosion of adjacent hillslopes during and after forest fires or large storm events, and (3) changes in hillslope sedimentation and water level due to rapid changes in climate and vegetation. We dismiss the first process because we see no evidence of landslide modification or old beaver dams near the outlet, and because it seems unlikely that outlet damming would induce the simultaneous deposition of colluvial sediments documented in our coring campaign. Hillslope erosion from nontectonic processes is less easy to dismiss, but our best evidence of a tectonic origin is the localization of the colluvial wedge deposits only along the anomalously E-W–trending northern margin of the marsh. We interpret the restriction of sand and pebbles to the bases of both wedge-shaped colluvial deposits as evidence that these sediments were shed from the adjacent hillsides rather than from flooding or high stream flow, which would likely distribute pulses of coarser sediment throughout the marsh. We interpret two other silty sand deposits in the lower parts of cores BO-1 and BO-04 (Fig. 10; Supplemental Fig. S6 [see footnote 6]) as probable examples of such fluvial processes, because both deposits thin toward the margin of the marsh. Both CE1 and CE2 (ca. 2 ka and ca. 8 ka, respectively; see discussion in "Earthquake Chronology" section) are roughly correlative with changes in regional climate (e.g., Galloway et al., 2009, their fig. 6), but we suspect that even the most rapid changes in climate would induce gradual changes in vegetation that would not cause the
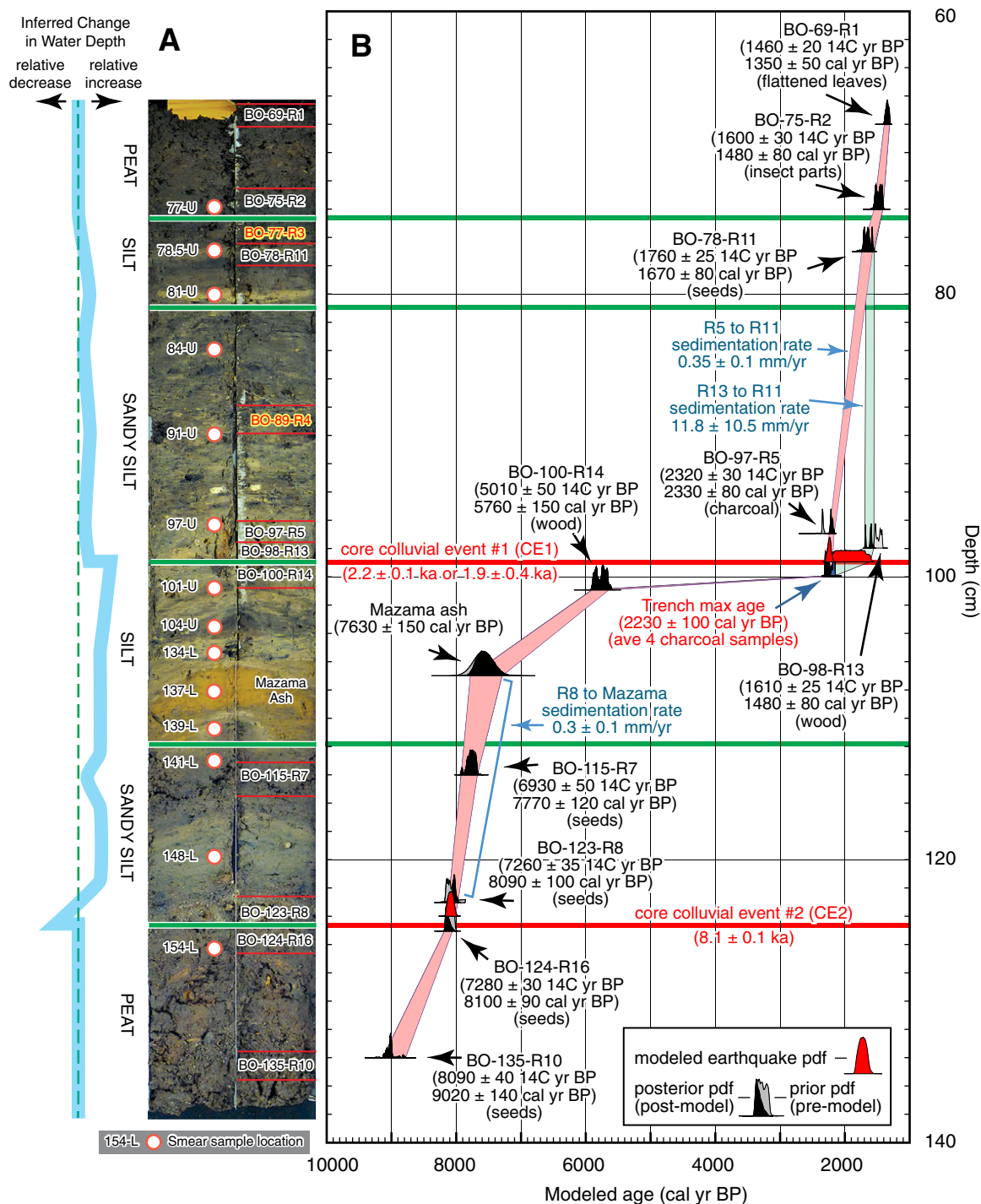
fied by road construction, but its height (6–8 m) suggested to us that it is probably a composite feature formed from glacial erosion along a preexisting fault zone and subsequent postglacial faulting. (2) Our analysis of the minimum constraints on the age of the CE1 colluvium in the marsh and the maximum constraints on the age of fault-scarp colluvium in the Springboard trench (LC1) indicates that both deposits are the same age and thus likely are related to a single surface-rupturing earthquake that occurred ca. 2 ka on this part of the Darrington–Devils Mountain fault zone (Table 1). (3) By analogy, we infer that similar sedimentologic characteristics of the younger (CE1) and older (CE2) colluvial deposits may indicate that both are related to surface-rupturing earthquakes. (4) Deposition of laminated silt beds and changes in diatom assemblages indicate that CE2 was followed by an abrupt deepening of the water level that

Figure 11. (A) Annotated photomosaic of two overlapping sections of larger-diameter (Russian) core BO-1, and inferred relative changes in water depth from qualitative evaluation of variations in sedimentation and diatom assemblages. Diatom sample locations (red-white circles) are shown on left side of photomosaic and described in Supplemental Figure S8 (see text footnote 8). Radiocarbon sample intervals (red lines) are shown on right side of photomosaic; ages not used in depth plot are denoted with red/yellow type. (B) OxCal (v. 4.2; Bronk Ramsey, 1995, 2008, 2009) depth plot of Boomer marsh sedimentation and inferred earthquake chronology based on radiocarbon ages from Aplodontia trench and marsh core BO-1. Heavy green horizontal lines are boundaries between major stratigraphic units. Heavy red horizontal lines mark abrupt incursions of colluvial sediment into the marsh that we interpret as evidence of earthquake surface ruptures. Shaded areas between probability density functions (pdfs) of chronologic data on the depth plot are our preferred (red) and alternative (green) models of sedimentation and surface faulting at the site.

abrupt and localized changes in hillslope erosion we infer from our coring data. However, shorter-term climate fluctuations, such as periods of extended drought, could cause nondeposition and soil formation near the margins of the marsh. We consider this origin unlikely, because desiccation should cause a "bathtub ring" with similar sedimentary characteristics around the perimeter of the wetland. Our reconnaissance coring shows that the southern margin exhibits highly variable sedimentation patterns that are strikingly different from those along the northern margin. In addition, the sharp lower contacts of both colluvial packages are inconsistent with soil formation and weathering of an emergent marsh surface.

DISCUSSION

Fault Geometry and Sense of Slip

The very steep fault dips exposed in the Lake Creek trenches are a significant source of uncertainty in our determination of the sense of slip on this reach of the Darrington–Devils Mountain fault zone. Depending on dip direction, the consistent north-side-up vertical separations apparent in all three trenches indicate either a component of normal displacement on a steeply south-dipping fault, or north-side-up reverse faulting on a steeply north-dipping fault. The latter scenario is supported by the apparent gentle anticlinal folding of the glacial sequence in the upthrown wall in the Aplodontia trench (Fig. 5), and it is consistent with north-south compression in the region (Mazzotti et al., 2002; Hyndman et al., 2003; Lewis et al., 2003). However, this scenario is at odds with Dragovich and DeOme's (2006, their cross-section B) interpretation of the Lake Creek scarps as graben structures in the hanging wall of their south-dipping "main strand." Given the modern stress regime and our doubt about the existence of their main strand, we suspect the fault zone is vertical or dips steeply to the north at depth. However, the possibility of triggered normal slip on upper-plate structures in Cascadia cannot be ruled out (Sherrod and Gomberg, 2014), because examples of large aftershocks with normal faulting mechanisms have occurred on favorably oriented upper-plate structures following recent subduction zone earthquakes in Chile (M8.8, 2010; Ryder et al., 2012) and Japan (M9.0, 2011; Kato et al., 2011). The angular relationship between the Darrington–Devils Mountain fault zone and the convergence direction of the Cascadia subduction zone is similar to some of the normal-slip aftershocks in the Chile and Japan sequences, so the Darrington–Devils Mountain fault zone may be favorably oriented

for extensional reactivation during great Cascadia earthquakes.

Three-dimensional trenching at the Aplodontia and Boundary excavations support our inference of a significant strike-skip component of faulting exposed in the original excavations (Figs. 8 and 9; Supplemental Figs. S4 and S5 [see footnotes 4 and 5]). This inference is consistent with previous studies that documented a component of left-lateral slip on parts of the fault zone (Johnson et al., 2001; Dragovich et al., 2004; Dragovich and DeOme, 2006). We also recognized that our main fault trace at the site makes a subtle right-stepping bend (Fig. 4B) that might accommodate localized extensional slip, but only if the strike-slip component is right-lateral.

At the Aplodontia trench, we excavated short slot trenches on both sides of and parallel to the main fault zone in the west wall of our original excavation (Fig. 8; Supplemental Fig. S4 [see footnote 4]). This wall was chosen because we recognized a linear piercing point in the east wall of the trench—the lateral edge of an apparent channel margin (unit 3b) ~1.5 m north of the main fault zone that was not exposed in the original west wall. Fortuitously, the southern slot trench exposed an identical channel margin in both walls of the slot trench. This line feature is subhorizontal and trends ~030°.

Projection of the channel margin observed in the east wall of the main trench at the same orientation to its intersection with the projection of the fault zone between the east and west walls yields a best estimate of 2.2 (+0.6, –1.0) m of right-lateral displacement of this piercing point. The listed uncertainties are likely maximum and minimum estimates based on two different projections of the channel between the east and west walls of the main trench.

Combined with the vertical separation of 45 cm of the unit 4–unit 3 contact across the fault zone in the east wall of the main trench (Fig. 5), and the 50 cm difference in elevation between the channel margins in the slot and main trenches (Fig. 5; Supplemental Fig. S4 [see footnote 4]), our lateral displacement measurement yields a horizontal-to-vertical ratio of ~5:1.

We also excavated a slot trench on the south side of and parallel to the main fault zone in the west wall of the Boundary trench. The only piercing point found in the original trench was a distinctive, ~30-cm-wide fault zone that juxtaposes weathered bedrock (unit 1) against highly sheared bedrock (unit 2) in the east wall of the trench (Fig. 9; Supplemental Fig. S5 [see footnote 5]). The bedrock fault zone projects across the floor of the main trench and intersects the west wall, where it is overprinted by shearing along the main fault zone. We exposed a similar

bedrock fault zone juxtaposing units 1 and 2 in the north and west walls of the slot trench that also indicates right-lateral slip. However, the bedrock fault zone in the slot trench consists of several strands that require at least two projections of possible piercing points. These projections yield an estimate of right-lateral slip (2.3 +0.5, –0.9 m) that is nearly identical to our estimate from the Aplodontia trench.

A second line of evidence for right-lateral oblique slip in the Aplodontia and Springboard trenches is the presence of numerous en echelon, subvertical fractures and secondary faults in glacial deposits in a 4- to 6-m-wide zone surrounding the main fault zones (Fig. 5). A similar set of fractures was mapped in a similar position in trench 1A by Puget Power (1974; Supplemental Fig. S2 [see footnote 2]). Most of these features have been disturbed by infiltration of small roots and groundwater. We mapped these features either as secondary faults where tiny (millimeter-scale) vertical offsets were visible in finely stratified glacial sediments, or as fractures where evidence of displacement could not be confirmed. For the former structures, the steep (~90°) dips and lack of consistent vertical offset directions suggest primarily strike-slip displacement. Orientations of all structures in the trenches were measured where the features were observed in the ~2-m-wide floors and both walls of the trenches (Supplemental Table S2A[10]).

Analysis of the secondary structures in the Aplodontia and Springboard trenches suggested to us that these features are Riedel shears for which orientations could be used to determine the lateral-slip direction of the main fault zone (Fig. 12). R shears form left-stepping, en echelon arrays along right-lateral shear zones, with orientations clockwise to the main shear zone. In contrast, R shears in left-lateral shear zones form right-stepping arrays with orientations counterclockwise to the main shear zone. In addition, Riedel theory predicts that R fractures should have synthetic shear and an angular difference from the main shear direction equal to $\phi/2$, where ϕ is the angle of internal friction of the faulted material. In contrast, R′ shears have antithetic shear and a much higher angular dif-

---

[10]Supplemental Table S2. Numerical data used to determine origin of Riedel shears in Aplodontia and Springboard trenches. See Figure 12 in text for graphic presentation of tabular results in this supplement. Table S2A. Fault- and fracture-orientation data from Aplodontia and Springboard trenches. Table S2B. Published data (Harp et al., 2008) from Seattle area used to estimate angle of internal friction (ϕ) of faulted sediments in Aplodontia and Springboard trenches. If you are viewing the PDF of this paper or reading it offline, please visit http://dx.doi.org/10.1130/GES01067.S10 or the full-text article on www.gsapubs.org to view Supplemental Table S2.

Figure 12. Structural data from Aplodontia and Springboard trenches: (A) Map of secondary faults and fractures (thin lines) and primary fault zones (thick lines) in Aplodontia and Springboard trenches, and (B) rose diagram (equal area, lower hemisphere) showing angular relationship between strikes of secondary faults and fractures, and primary fault zones in Aplodontia and Springboard trenches. See Supplemental Table S2 (see text footnote 10) for data and calculations used in the analysis.
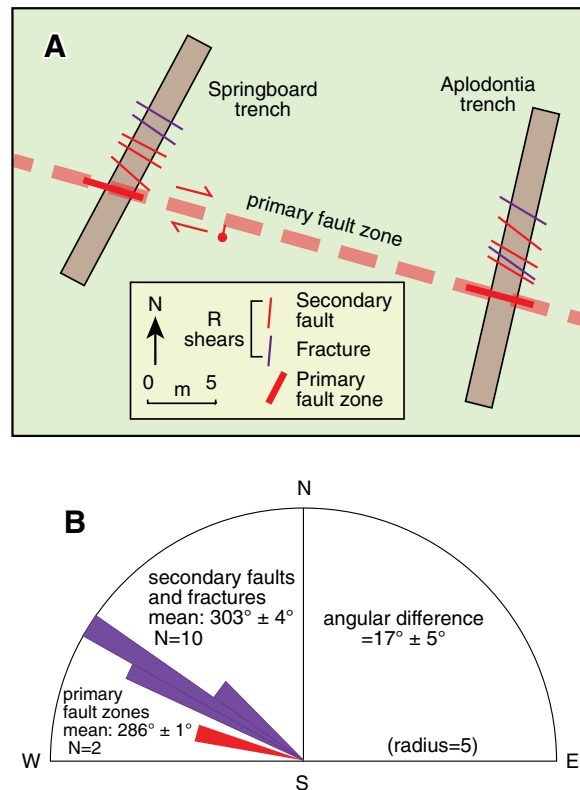
ference (90° – ϕ/2) from the main shear direction (Riedel, 1929; Tchalenko, 1968, 1970). If our secondary structures are R shears rather than R′ shears, then their orientation indicates right-lateral slip on the Lake Creek portion of the Darrington–Devils Mountain fault zone. We used eight values of ϕ of Vashon-aged glacial deposits from a compilation of values for Quaternary sediments in the Seattle area (Harp et al., 2008, their table 1) to estimate ϕ for the faulted glacial sediments at the Lake Creek site (Supplemental Table S2B [see footnote 10]). These eight values range from 24° to 38° and yield average values of 32° ± 5° (mean), 33° (median), or 34° (mode). Thus, the theoretical angular difference for R shears in average Vashon glacial deposits is 32°–34°/2 = 16°–17° ± 5°. The attitudes of mapped fractures and shears in the Aplodontia and Springboard trenches (mean strike of 303°, *n* = 10), and the average strike of the main fault zone (286°, *n* = 2) yield an actual angular difference in strike (17° ± 5°) that is nearly identical to the theoretical values calculated from the estimated internal angle of friction of the faulted sediments in the trenches (Fig. 12). In contrast, if the fractures and faults were R′ shears, then their predicted strike difference would be 73° ± 5°. No fractures or shears with such orientations were observed in any of our Lake Creek trenches, so we conclude that the secondary structures are Riedel R shears. Although the mapped lengths

of the R shears in our excavations are too short (~2 m) to discern clear stepping patterns, these shears are clearly oriented clockwise to the main shear direction (Fig. 12) and thus are indicative of right-lateral displacement.

The orientation of slickensides observed in the Boundary trench constitutes a third line of evidence for a significant component of lateral displacement on the Darrington–Devils Mountain fault zone in the late Quaternary. We interpret the western plunge of slickenlines in sheared bedrock along the western primary fault and clear evidence of north-side-up vertical separation of trench units and fault scarps as evidence of right-lateral oblique slip during at least one surface-rupturing earthquake (Fig. 7). In addition, the two slickenside measurements in glacial sediments on the eastern primary fault indicate nearly pure strike-slip displacement. The significance of the differences in orientation of these two sets of slickensides is unknown, but the indicators of nearly pure strike slip may be evidence of a second post–last-glacial earthquake with significantly less vertical displacement. The lack of evidence for a significant increase in water depth associated with the youngest colluvial event (CE1) in the BO-1 core (Fig. 11A) indicates that CE1 may have been accompanied by less vertical offset than event CE2. Given the evidence for both pure strike-slip and oblique-slip postglacial sur-

face faulting, we conclude that the most robust method of calculating a net post–last-glacial slip vector is to use the combined slip and fault orientation data from the Lake Creek trench site. We used the averages of the displacement measurements from the Aplodontia and Boundary trenches (2.25 ± 1.1 m right-lateral and 0.6 ± 0.1 m north-side-up vertical) and fault orientation data (strike 286°, dip 90°) to determine a net slip vector of 2.3 ± 1.1 m plunging 14° west.

Our preferred interpretation of right-lateral, north-side-up oblique slip on a vertical to steeply north-dipping fault zone is exactly opposite the sense of slip determined for the Lake Creek site by Dragovich and DeOme (2006). The reversal of shear direction is difficult to explain (see discussion in "Regional Implications" section), but we suspect that the differences in sense of vertical slip are likely due to minor variations in dip angle along strike of the near-vertical Darrington–Devils Mountain fault zone. Although generally mapped as south-side-up, recent quadrangle mapping in the region shows evidence of both north-side-up and south-side-up senses of Quaternary slip along the central Darrington–Devils Mountain fault zone. For example, 10 km east of the Lake Creek site, an anomalous increase in gradient (Dragovich and DeOme, 2006, their fig. 3) and the presence of uplifted(?) Holocene terraces (Dragovich et al., 2004) on Pilchuck Creek north of the mapped trace of the Darrington–Devils Mountain fault zone indicate north-side-up slip, but 8–10 km further east, Dragovich et al. (2004) showed their "main strand" offsetting the lake bottom south-side-up beneath Lake Cavanaugh. Still further east, between Deer Creek and Stillaguamish River, cross sections based on water well data (Dragovich et al., 2003a, 2003b) suggest north-side-up offsets of Olympia-aged (>20–60 ka) interglacial and older (pre-Vashon) glacial sediments along the Darrington–Devils Mountain fault zone. Such changes in apparent vertical slip direction along strike are a classic characteristic of strike-slip fault systems (e.g., Sylvester, 1988).

Earthquake Chronology

We used accelerator mass spectrometry (AMS) radiocarbon dating of charcoal, wood, and macrofossil plant and animal remains from our trench and coring investigations (Table 1) to constrain the ages of two possible surface-rupturing earthquakes on the Darrington–Devils Mountain fault zone at the Lake Creek site. To calibrate the laboratory-reported ages and put them in stratigraphic context, we constructed a combined depth model (Fig. 11B) in OxCal (v. 4.2; Bronk Ramsey, 1995, 2008, 2009), using

the IntCal09 calibration curve of Reimer et al. (2009). OxCal uses Bayesian analysis of prior information such as laboratory uncertainties and stratigraphic relationships, along with the likelihood (represented by probability distribution functions or PDFs) of each age determination, to estimate the ages of undated events, in our case, prehistoric earthquakes.

We used a combination of ages from our trench and coring investigations to estimate the time of the most recent earthquake (MRE) on this part of the Darrington–Devils Mountain fault zone. The mean of four nearly identical charcoal ages from the Springboard trench provides a close maximum age of the MRE (LC1), based on the location of samples from a buried soil directly beneath fault scarp colluvial deposits and from a burned root faulted during the earthquake (Fig. 5; Supplemental Fig. S3 [see footnote 3]). No minimum ages for the trench MRE were obtained, so we used our correlation of earthquake LC1 with colluvial event CE1 (see previous discussion) to justify the addition of the charcoal ages from the trench to an OxCal depth plot of ages from core BO-1 to better constrain the time of the LC1/CE1 earthquake. The minimum time of this event is constrained by two somewhat conflicting ages, charcoal sample BO-97-R5 (2330 ± 80 cal. yr B.P.) from a core depth of 97 cm, and wood sample BO-98-R13 (1480 ± 80 cal. yr B.P.) from a core depth of 98 cm (directly above the CE1 unconformity). We have reason to suspect both of these samples: The older charcoal sample likely has some inherited age (e.g., Gavin, 2001), as suggested by the ~200–1100 yr inheritance for the two other charcoal samples from the core (Table 1), and the younger wood age, which is younger than (and does not overlap with at 2σ uncertainties) the likely more accurate age on seed sample BO-78-R11 (1670 ± 80 cal. yr), which lies 20 cm higher in the core. Although the charcoal age (2330 ± 80 cal. yr B.P.) may be a few hundred years too old, we prefer this age because it yields a post-CE1 sedimentation rate (~0.35 mm/yr) that is nearly identical to the pre-Mazama-ash rate (~0.3 mm/yr), rather than the anomalously fast post-CE1 rate (~12 mm/yr) inferred from the stratigraphically inverted wood age (Fig. 11B). Our OxCal models using the charcoal and wood minimum ages yielded modeled timing estimates of LC1/CE1 of 2.2 ± 0.1 ka and 1.9 ± 0.4 ka, respectively (Fig 11B). Given the concerns we have about both of the minimum constraints, we consider 2.3–1.5 ka (1.9 ± 0.4 ka) to be a reasonable estimate of the 2σ time range for this earthquake.

Evidence for an earthquake origin for colluvial event CE2 is much more equivocal, but in contrast to the uncertainties surrounding the timing of the LC1/CE1 earthquake, radiocarbon ages on seeds sampled directly above and below the CE2 unconformity (Fig. 11A; Supplemental Fig. S7 [see footnote 7]) yield a tightly constrained model time estimate of 8.1 ± 0.1 ka (2σ) for this possible penultimate earthquake.

Paleoearthquake Parameters

Calculations of prehistoric earthquake magnitudes are commonly based on estimates of surface-rupture length and displacement (e.g., Wells and Coppersmith, 1994). Estimating surface-rupture length is especially difficult in the heavily vegetated Pacific Northwest. We follow Dragovich and DeOme (2006) in mapping fault scarps in glacial deposits in the Lake Creek area, but these scarps are only ~1 km long and likely were part of a much longer surface rupture or ruptures that are now obscured by vegetation and steep slopes in the foothills of the Cascade Range. We estimate a minimum surface-rupture length of ~30 km, from the prominent bedrock lineaments on the south flank of Devils Mountain west of Lake Creek, through Lake Cavanaugh, where Holocene lake bottom sediments are apparently offset in reflection profiles, to the vicinity of Deer Creek, where Dragovich et al. (2003b) noted the "probable displacement of Quaternary strata" along a subsidiary fault (Fig. 3). This minimum surface-rupture length yields estimates of Mw of >6.8 (Wells and Coppersmith, 1994; all faults data set), >6.8 (Wesnousky, 2008; all faults data set), and >7.0 (Stirling et al., 2002; average of instrumental and preinstrumental data sets). Calculations of prehistoric earthquake magnitudes based on estimates of surface displacement are complicated by uncertainties about whether the displacement estimates are average or maximum values, as well as the number of earthquakes responsible for our displacement values. In our preferred scenario (two earthquakes), one half of our preferred displacement value of 2.3 ± 1.1 m (1.15 m) yields an estimated Mw of 7.0; if our preferred displacement value is a maximum, then it yields an estimated Mw of 6.7 (Wells and Coppersmith, 1994; all faults data sets). Alternatively, if our preferred displacement value is the result of a single earthquake, then the same empirical relations yield magnitude estimates of Mw of 7.2 (average slip) and Mw 7.0 (maximum slip).

We can also use our average displacement and surface-rupture length values, an estimated seismogenic depth of 15 km, and a dip of 90° to calculate moment magnitude using the area/magnitude relation of Hanks and Kanamori (1979). This relation yields estimates of Mw 6.8 (two earthquakes) and Mw 7.0 (one earthquake). We conclude that the past surface-rupturing earthquakes were likely Mw 6.7–7.0, and they produced strong ground shaking in the region.

Our trench and coring studies produced a record of one and possibly two paleoearthquakes on the central Darrington–Devils Mountain fault zone since deglaciation of the Puget Lowland in the latest Pleistocene. These two possible earthquakes, dated at 1.9 ± 0.4 ka and 8.1 ± 0.1 ka, yield a single recurrence interval of ~6 k.y., and an elapsed time (open interval) of ~2 k.y. since the MRE. We measured 2.3 ± 1.1 m of right-lateral oblique slip postdating deglaciation of the Lake Creek site, which we infer was ice-free by ca. 16 ± 0.5 ka (e.g., Dethier et al., 1995; Porter and Swanson, 1998). These data yield an average postglacial slip rate of 0.14 ± 0.1 mm/yr. We consider this a minimum rate because of the unknown (but likely small) contribution of slip from the untrenched southern strand and possibly from other unmapped fault traces, and uncertainties related to our reliance on slip values from a single paleoseismic site.

Regional Implications

Despite its length and geologic longevity, our results indicate lower rates of paleoseismic activity on the Darrington–Devils Mountain fault zone than several less prominent Holocene-active faults in the northern Puget Lowland. For instance, the Sandy Point fault in the Bellingham Basin (Fig. 1B) has generated three earthquakes resulting in coseismic uplift of ~4 m in the last 6 k.y. (Kelsey et al., 2012). In the northeast corner of the Bellingham Basin, the Boulder Creek fault has experienced at least three surface-rupturing earthquakes in the last 8 k.y. and has a postglacial vertical slip rate of 0.3–0.6 mm/yr (Sherrod et al., 2013). The Utsalady Point fault in the northwest corner of the Everett Basin (Fig. 1B) has probably experienced two postglacial surface-rupturing earthquakes, but both occurred in the last 2.2 k.y. and were accompanied by larger surface displacements: One trench showed evidence of two earthquakes that totaled as much as 4.5 m of vertical separation, and a second trench showed evidence of one earthquake that totaled 1–1.5 m of vertical and ~2 m of lateral slip (Johnson et al., 2004). Although the apparently low rate of Holocene paleoseismicity on the Darrington–Devils Mountain fault zone may be attributable to an incomplete paleoseismic record, we believe our recurrence and slip rates from the Lake Creek site are consistent with the dispersed and subdued expression of postglacial rupture along the mapped trace of the Darrington–Devils Mountain fault zone.

Comparisons of regional paleoearthquake histories also raise questions about the possibility of clustering of Darrington–Devils Mountain fault zone paleoearthquakes with earthquakes on other crustal faults in the region, as well as the potential for triggering crustal earthquakes by great earthquakes on the Cascadia subduction zone (e.g., Sherrod and Gomberg, 2014). Several regional structures have dated earthquakes with ages similar to the youngest earthquake on the Darrington–Devils Mountain fault zone, such as the Sandy Point fault (ca. 2.1 ka; Kelsey et al., 2012), the Utsalady fault (2.1–1.2 ka; Johnson et al., 2004), the Seattle fault (2.6–1.9 ka; Nelson et al., 2003a, 2014), and the Lake Creek–Boundary Creek fault (2.0–0.6 ka; Nelson et al., 2007). However, neither the Darrington–Devils Mountain fault zone nor the regional earthquake time estimates are precise enough for us to confidently correlate these earthquakes with one another or with a great earthquake on the Cascadia subduction zone.

The occurrence of the devastating 22 March 2014 landslide along the south flank of the Whitman bench has drawn attention to the numerous older landslides mapped in the immediate area (Dragovich et al., 2003a, 2003b; Haugerud, 2014). The 2014 landslide was not seismically induced (B.W. Presgrave, U.S. Geological Survey, 2014, written commun.), but given the inherent instability of steep slopes along the bench, we speculate that large earthquakes such as our ca. 2 ka LC1/CE1 event on the Darrington–Devils Mountain fault zone might have triggered some of the older landslides in the area. Confirmation of a seismic origin must await future studies on the ages of the older landslide deposits, but the proximity of the Darrington–Devils Mountain fault zone to unstable slopes along the Whitman bench should be taken into account in future assessments of landslide hazards in the region.

One of the more curious aspects of our results is the evidence for right-lateral oblique displacement on what has previously been described as primarily a left-lateral reverse structure (Johnson et al., 2001; Dragovich and DeOme, 2006). Because the modern stress field is dominated by the rapid (>40 mm/yr) oblique subduction of the Juan de Fuca plate beneath the region, current geodetic techniques may be of limited use in determining slip sense and rates on crustal faults with much lower (<1 mm/yr) rates of slip (McCaffrey et al., 2013). However, most seismicity studies indicate N-S–directed compression in the Puget Lowland (Ma et al., 1996; Mazzotti et al., 2002; Van Wagoner et al., 2002; Hyndman et al., 2003; Lewis et al., 2003). Seismicity along the Darrington–Devils Mountain fault zone is sparse (Figs. 1B and 3), and

only a handful of focal mechanisms from small (Mw <4) earthquakes near the Darrington–Devils Mountain fault zone have been published (Zollweg and Johnson, 1989; Ma et al., 1996; Van Wagoner et al., 2002). We used the structural grain visible on published geologic maps (Dragovich et al., 2002a, 2002b, 2002c, 2003a, 2004; Dragovich and DeOme, 2006) near the projected surface locations of the two possible fault planes to select preferred fault plane orientations from five of these mechanisms (Fig. 3). Although we do not know if these earthquakes occurred on the Darrington–Devils Mountain fault zone, their likely orientations primarily indicate reverse oblique displacement on near-vertical to steeply north-dipping, roughly E-W–striking fault planes. Such orientations are consistent with regional N-S compression. Two of the focal mechanisms from Van Wagoner et al. (2002) also indicate a small component of right-lateral oblique slip, and, as noted by Van Wagoner et al. (2002), these mechanisms are not consistent with a left-lateral slip component on the Darrington–Devils Mountain fault zone as proposed in previous studies (e.g., Johnson et al., 2001; Dragovich and DeOme, 2006). We reiterate that the relationship between these small-magnitude earthquakes and the Darrington–Devils Mountain fault zone is unknown, but the very limited focal mechanism data are at least supportive of our interpretation of Holocene right-lateral slip on the central part of the Darrington–Devils Mountain fault zone.

The cause of the apparent slip reversal is unknown, but aspects of local and regional tectonic controls provide some potential explanations. One possible explanation is that the Lake Creek scarps are located on one of several right-lateral, northwest-striking faults that intersect the Darrington–Devils Mountain fault zone in the vicinity of our Lake Creek site (Dragovich and DeOme, 2006), rather than being located on the Darrington–Devils Mountain fault zone itself. One such structure is mapped as intersecting the Darrington–Devils Mountain fault zone in the western end of the Boomer marsh (Fig. 4). This alternative does not require any change in slip direction, but it is not supported by (1) the abundant evidence of late Quaternary slip elsewhere along the main trace of the Darrington–Devils Mountain fault zone, (2) our evidence for surface faulting along the northern margin of Boomer marsh, and (3) the lack of any evidence for Quaternary displacement elsewhere along the NW-striking bedrock faults. Another possible, and perhaps more likely, explanation is that clockwise rotation of the North Cascadia block (Wells et al., 1998; McCaffrey et al., 2007) has reoriented the Darrington–Devils Mountain fault zone to a more northwesterly

strike that is slightly more favorable to a right-lateral component of slip in the current N-S compressive stress field. A recent comparison of paleomagnetic and geodetic rotation rates in the northwestern United States indicates that the Puget Lowland is currently rotating clockwise at a rate of ~0.5 mm/yr, and it has rotated as much as 6°–7° in the last 12 m.y. (McCaffrey et al., 2013; Wells and McCaffrey, 2013). However, more detailed study will be required to document if this progressive change in orientation was large enough to change the sense of slip of the Darrington–Devils Mountain fault zone, and when such a change might have occurred.

CONCLUSIONS

We used the results of three-dimensional trenching of a prominent fault scarp and coring of an adjacent wetland to compile a composite Holocene history of surface-rupturing earthquakes on the Darrington–Devils Mountain fault zone at the Lake Creek site southeast of Mount Vernon, Washington. Trenching revealed evidence of extensive biogenic disruption of the upper 50–100 cm of our exposures, but radiocarbon dating of charcoal from a single preserved deposit of fault-scarp colluvium indicates at least one large earthquake ruptured through the site ca. 2 ka. In the adjacent wetland, we interpret the presence of two basinward-thinning silty colluvial deposits along our inferred trace of the Darrington–Devils Mountain fault zone as evidence of two possible earthquakes, one coincident with the timing of the earthquake documented in the trenches ca. 2 ka, and an earlier possible earthquake ca. 8 ka. Slip components determined from faulted glacial deposits (2.25 ± 1.1 m right-lateral and 0.6 ± 0.1 m north-side-up vertical) yield a right-lateral oblique net slip of 2.3 ± 1.1 m plunging 14° west on a vertical fault striking 286°, and a postglacial minimum slip rate of 0.14 ± 0.1 mm/yr. Individual displacements could not be determined, but if each earthquake accounted for about half of the net slip, then empirical relations based on historical surface faulting indicate magnitudes of Mw 6.7–7.0. The timing of these two possible earthquakes yields a single recurrence interval of ~6 k.y., and an elapsed time (open interval) of ~2 k.y. since the most recent earthquake. A single recurrence interval is insufficient to quantify the probability of future seismic activity on the fault zone, but the occurrence of at least one and possibly two surface-rupturing earthquakes in the middle and late Holocene indicate the Darrington–Devils Mountain fault zone is a potential source of future large (Mw 6.7–7.0) earthquakes in northwestern Washington.

REFERENCES CITED

Adair, M.J., Talmage, R.H., Crosby, T.W., and Testa, S.M., 1989, Geology and seismicity of the Skagit Nuclear Power Plant site, *in* Galster, R.W., chairman, Engineering Geology in Washington: Washington Division of Geology and Earth Resources Bulletin 78, v. I, p. 607–624.

Barnett, E.A., Haugerud, R.A., Sherrod, B.L., Weaver, C.S., Pratt, T.L., and Blakely, R.J., 2010, Preliminary Atlas of Active Shallow Tectonic Deformation in the Puget Lowland, Washington: U.S. Geological Survey Open-File Report 2010–1149, 32 p.

Bechtel, Inc., 1979, Report of Geologic Investigations in 1978–1979; Skagit Nuclear Power Project: Puget Sound Power and Light Company, 3 volumes, 3 plates, variously paginated.

Blakely, R.J., Sherrod, B.L., Hughes, J.F., Anderson, M.L., Wells, R.E., and Weaver, C.S., 2009, Saddle Mountain fault deformation zone, Olympic Peninsula, Washington: Western boundary of the Seattle Uplift: Geosphere, v. 5, p. 105–125, doi:10.1130/GES00196.1.

Brocher, T.M., Parsons, T., Blakely, R.J., Christensen, N.I., Fisher, M.A., Wells, R.E., and the SHIPS Working Group, 2001, Upper crustal structure in Puget Lowland, Washington: Results from the 1998 seismic hazard investigation in Puget Sound: Journal of Geophysical Research, v. 106, no. B7, p. 13,541–13,564, doi:10.1029/2001JB000154.

Bronk Ramsey, C., 1995, Radiocarbon calibration and analysis of stratigraphy: The OxCal program: Radiocarbon, v. 37, no. 2, p. 425–430.

Bronk Ramsey, C., 2008, Deposition models for chronological records: Quaternary Science Reviews, v. 27, p. 42–60, doi:10.1016/j.quascirev.2007.01.019.

Bronk Ramsey, C., 2009, Bayesian analysis of radiocarbon dates: Radiocarbon, v. 51, no. 1, p. 337–360.

Bucknam, R.C., Hemphill-Haley, E., and Leopold, E.B., 1992, Abrupt uplift within the past 1,700 years at southern Puget Sound, Washington: Science, v. 258, no. 5088, p. 1611–1614, doi:10.1126/science.258.5088.1611.

Bucknam, R.C., Sherrod, B.L., and Elfendahl, G.W., 1999, A fault scarp of probable Holocene age in the Seattle fault zone, Bainbridge Island, Washington: Seismological Research Letters, v. 258, p. 1611–1614.

Crosby, T.W., Talmage, R.H., and Adair, M.J., 1986, Radiocarbon dating and geomorphic evidence for dating movement on the Devils Mountains fault zone, northwestern Washington: Geological Society of America Abstracts with Programs, v. 18, no. 2, p. 97.

David, P.P., 1970, Discovery of Mazama ash in Saskatchewan, Canada: Canadian Journal of Earth Sciences, v. 7, p. 1579–1583, doi:10.1139/e70-150.

Dethier, D.P., Pessl, F., Jr., Keuler, R.F., Balzarini, M.A., and Pevear, D.R., 1995, Late Wisconsinan glaciomarine deposition and isostatic rebound, northern Puget Low-

land, Washington: Geological Society of America Bulletin, v. 107, no. 11, p. 1288–1303, doi:10.1130/0016-7606(1995)107<1288:LWGDAI>2.3.CO;2.

Dragovich, J.D., and DeOme, A.J., 2006, Geologic Map of the McMurray 7.5-Minute Quadrangle, Skagit and Snohomish Counties, Washington, with a Discussion of the Evidence for Holocene Activity on the Darrington–Devils Mountain Fault Zone: Washington Division of Geology and Earth Resources Geologic Map GM-61, scale 1:24,000, 1 sheet, 18 p. text.

Dragovich, J.D., Gilbertson, L.A., Lingley, W.S., Jr., Polenz, M., and Glenn, J., 2002a, Geologic Map of the Darrington 7.5-Minute Quadrangle, Skagit and Snohomish Counties, Washington: Washington Division of Geology and Earth Resources Open-File Report 2002-7, scale 1:24,000, 1 sheet.

Dragovich, J.D., Gilbertson, L.A., Lingley, W.S., Jr., Polenz, M., and Glenn, J., 2002b, Geologic Map of the Fortson 7.5-Minute Quadrangle, Skagit and Snohomish Counties, Washington: Washington Division of Geology and Earth Resources Open-File Report 2002-6, scale 1:24,000, 1 sheet.

Dragovich, J.D., Gilbertson, L.A., Norman, D.K., Anderson, G., and Petro, G.T., 2002c, Geologic Map of the Utsalady and Conway 7.5-Minute Quadrangles, Skagit, Snohomish, and Island Counties, Washington, Revised 2004: Washington Division of Geology and Earth Resources Open-File Report 2002-5, scale 1:24,000, 2 sheets, 34 p.

Dragovich, J.D., Stanton, B.W., Lingley, W.S., Jr., Griesel, G.A., and Polenz, M., 2003a, Geologic Map of the Mount Higgins 7.5-Minute Quadrangle, Skagit and Snohomish Counties, Washington: Washington Division of Geology and Earth Resources Open-File Report 2003-12, scale 1:24,000, 1 sheet.

Dragovich, J.D., Stanton, B.W., Lingley, W.S., Jr., Griesel, G.A., and Polenz, M., 2003b, Geologic Map of the Oso 7.5-Minute Quadrangle, Skagit and Snohomish Counties, Washington: Washington Division of Geology and Earth Resources Open-File Report 2003-11, scale 1:24,000, 1 sheet.

Dragovich, J.D., Wolfe, M.W., Stanton, B.W., and Norman, D.K., 2004, Geologic Map of the Stimson Hill 7.5-Minute Quadrangle, Skagit and Snohomish Counties, Washington: Washington Division of Geology and Earth Resources Open-File Report 2004-9, scale 1:24,000, 1 sheet.

Dragovich, J.D., Petro, G.T., Thorsen, G.W., Larson, S.L., Foster, G.R., and Norman, D.K., 2005, Geologic Map of the Oak Harbor, Crescent Harbor, and Part of the Smith Island 7.5-Minute Quadrangles, Island County, Washington: Washington Division of Geology and Earth Resources Geologic Map GM-59, scale 1:24,000, 2 sheets.

Flower, R.J., and Ryves, D.B., 2009, Diatom preservation: Differential preservation of sedimentary diatoms in two saline lakes: Acta Botanica Croatica, v. 68, no. 2, p. 381–399.

Galloway, J.M., Doherty, C.T., Patterson, R.T., and Roe, H.M., 2009, Postglacial vegetation and climate dynamics in the Seymour–Belize Inlet Complex, central coastal British Columbia, Canada: Palynological evidence from Tiny Lake: Journal of Quaternary Science, v. 24, p. 322–335, doi:10.1002/jqs.1232.

Gavin, D.G., 2001, Estimation of inbuilt age in radiocarbon ages of soil charcoal for fire history studies: Radiocarbon, v. 43, no. 1, p. 27–44.

Hanks, T.C., and Kanamori, H., 1979, A moment magnitude scale: Journal of Geophysical Research, v. 84, no. B5, p. 2348–2350, doi:10.1029/JB084iB05p02348.

Harding, D.J., and Berghoff, G.S., 2000, Fault scarp detection beneath dense vegetation cover: Airborne LIDAR mapping of the Seattle fault zone, Bainbridge Island, Washington State, *in* Proceedings of the American Society of Photogrammetry and Remote Sensing Annual Conference, May, 2000: Washington, D.C., American Society of Photogrammetry and Remote Sensing, 11 p., http://pugetsoundlidar.ess.washington.edu/harding.pdf.

Harp, E.L., Michael, J.A., and Laprade, W.T., 2008, Shallow landslide hazard map of Seattle, Washington, *in* Baum, R.L., Godt, J.W., and Highland, L.M., eds., Landslides and Engineering Geology of the Seattle, Washington, Area: Geological Society of America Reviews in Engi-

neering Geology, v. 20, p. 67–82, doi:10.1130/2008.4020(04).

Haugerud, R.A., 2014, Preliminary Interpretation of Pre-2014 Landslide Deposits in the Vicinity of Oso, Washington: U.S. Geological Survey Open-File Report 2014–1065, 4 p., http://dx.doi.org/10.3133/ofr20141065.

Haugerud, R.A., Harding, D.J., Johnson, S.Y., Harless, J.L., and Weaver, C.S., 2003, High-resolution LIDAR topography of the Puget Lowland, Washington—A bonanza for Earth science: GSA Today, v. 13, no. 6, p. 4–10, doi:10.1130/1052-5173(2003)13<0004:HLTOTP>2.0.CO;2.

Hayward, N., Nedimović, M.R., Cleary, M., and Calvert, A.J., 2006, Structural variation along the Devil's Mountain fault zone, northwestern Washington: Canadian Journal of Earth Sciences, v. 43, p. 433–446, doi:10.1139/e06-002.

Hyndman, R.D., Mazzotti, S., Weichert, D., and Rogers, G.C., 2003, Frequency of large crustal earthquakes in Puget Sound–southern Georgia Strait predicted from geodetic and geological deformation rates: Journal of Geophysical Research, v. 108, no. B1, p. 2033, doi:10.1029/2001JB001710.

Johnson, S.Y., Potter, C.J., Armentrout, J.M., Miller, J.J., Finn, C., and Weaver, C.S., 1996, The southern Whidbey Island fault: An active structure in the Puget Lowland, Washington: Geological Society of America Bulletin v. 108, no. 3, p. 334–354 and oversize insert, doi:10.1130/0016-7606(1996)108<0334:TSWIFA>2.3.CO;2.

Johnson, S.Y., Dadisman, S.V., Childs, J.R., and Stanley, W.D., 1999, Active tectonics of the Seattle fault and central Puget Sound, Washington—Implications for earthquake hazards: Geological Society of America Bulletin, v. 111, no. 7, p. 1042–1053, doi:10.1130/0016-7606(1999)111<1042:ATOTSF>2.3.CO;2.

Johnson, S.Y., Dadisman, S.V., Mosher, D.C., Blakely, R.J., and Childs, J.R., 2001, Active Tectonics of the Devils Mountain Fault And Related Structures, Northern Puget Lowland and Eastern Strait of Juan de Fuca Region, Pacific Northwest: U.S. Geological Survey Professional Paper 1643, 45 p., 2 plates.

Johnson, S.Y., Nelson, A.R., Personius, S.F., Wells, R.E., Kelsey, H.M., Sherrod, B.L., Okumura, K., Koehler, R., III, Witter, R.C., Bradley, L.-A., and Harding, D.J., 2004, Evidence for late Holocene earthquakes on the Utsalady Point fault, northern Puget Lowland, Washington: Bulletin of the Seismological Society of America, v. 94, no. 6, p. 2299–2316, doi:10.1785/0120040050.

Kato, A., Sakai, S., and Obara, K., 2011, A normal-faulting seismic sequence triggered by the 2011 off the Pacific coast of Tohoku earthquake: Wholesale stress regime changes in the upper plate: Earth, Planets, and Space, v. 63, p. 745–748, doi:10.5047/eps.2011.06.014.

Kelsey, H.M., Sherrod, B.L., Nelson, A.R., and Brocher, T.M., 2008, Earthquakes generated from bedding-plane–parallel reverse faults above an active wedge thrust, Seattle fault zone: Geological Society of America Bulletin, v. 120, no. 11–12, p. 1581–1597, doi:10.1130/B26282.1.

Kelsey, H.M., Sherrod, B.L., Blakely, R.J., and Haugerud, R.A., 2012, Holocene faulting in the Bellingham forearc basin: Upper-plate deformation at the northern end of the Cascadia subduction zone: Journal of Geophysical Research, v. 117, B03409, doi:10.1029/2011JB008816.

Lewis, J.C., Unruh, J.R., and Twiss, R.J., 2003, Seismogenic strain and motion of the Oregon coast block: Geology, v. 31, no. 2, p. 183–186, doi:10.1130/0091-7613(2003)031<0183:SSAMOT>2.0.CO;2.

Loveseth, T.P., 1975, The Devils Mountain Fault Zone, Northwestern Washington [M.S. thesis]: Seattle, Washington, University of Washington, 29 p.

Ma, L., Crosson, R.S., and Ludwin, R.S., 1996, Western Washington earthquake focal mechanisms and their relationship to regional tectonic stress, *in* Rogers, A.M., Walsh, T.J., Kockelman, W.J., and Priest, G.R., eds., Assessing Earthquake Hazards and Reducing Risk in the Pacific Northwest: U.S. Geological Survey Professional Paper 1560, v. 1, p. 257–283.

Mace, C.G., and Keranen, K.M., 2012, Oblique fault systems crossing the Seattle Basin: Geophysical evidence for additional shallow fault systems in the central Puget

Lowland: Journal of Geophysical Research, v. 117, B03105, doi:10.1029/2011JB008722.

Mazzotti, S., Dragert, H., Hyndman, R.D., Miller, M.M., and Henton, J.A., 2002, GPS deformation in a region of high crustal seismicity: N. Cascadia forearc: Earth and Planetary Science Letters, v. 198, p. 41–48, doi:10 .1016/S0012-821X(02)00520-4.

McCaffrey, R.A., Qamar, A.I., King, R.W., Wells, R.E., Khazaradze, G., Williams, C.A., Stevens, C.W., Vollick, J.J., and Zwick, P.C., 2007, Fault locking, block rotation and crustal deformation in the Pacific Northwest: Geophysical Journal International, v. 169, p. 1315–1340, doi:10.1111/j.1365-246X.2007.03371.x.

McCaffrey, R.A., King, R.W., Payne, S.J., and Lancaster, M., 2013, Active tectonics of northwestern U.S. inferred from GPS-derived surface velocities: Journal of Geophysical Research, v. 118, p. 709–723, doi:10 .1029/2012JB009473.

Naugler, W.E., Karlin, R.E., and Holmes, M.L., 1996, Lakes as windows in the crust—Lake Cavanaugh and the Devils Mountain fault, northwestern Washington: Geological Society of America Abstracts with Programs, v. 28, no. 5, p. 95.

Nelson, A.R., Johnson, S.Y., Kelsey, H.M., Wells, R.E., Sherrod, B.L., Pezzopane, S.K., Bradley, L.-A., Koehler, R.D., III, and Bucknam, R.C., 2003a, Late Holocene earthquakes on the Toe Jam Hill fault, Seattle fault zone, Bainbridge Island, Washington: Geological Society of America Bulletin, v. 115, no. 11, p. 1388–1403, doi:10.1130/B25262.1.

Nelson, A.R., Johnson, S.Y., Kelsey, H.M., Sherrod, B.L., Wells, R.E., Okumura, K., Bradley, L.-A., Bogar, R., and Personius, S.F., 2003b, Field and Laboratory Data from an Earthquake History Study of the Waterman Point Fault, Kitsap County, Washington: U.S. Geological Survey Miscellaneous Field Studies Map MF-2423, 1 plate, http://pubs.usgs.gov/mf/2003/mf-2423/.

Nelson, A.R., Personius, S.F., Buck, J., Bradley, L.-A., Wells, R.E., and Schermer, E.R., 2007, Field and Laboratory Data from an Earthquake History Study of Scarps of the Lake Creek–Boundary Creek Fault between the Elwah River and Siebert Creek, Clallam County, Washington: U.S. Geological Survey Scientific Investigations Map 2961, 2 plates, http://pubs.er.usgs.gov/usgspubs/sim /sim2961.

Nelson, A.R., Personius, S.F., Buck, J., Bradley, L.-A., Sherrod, B.L., Henley, G., II, Liberty, L.M., Kelsey, H.M., Witter, R.C., Koehler, R.D., III, and Schermer, E.R., 2008, Field and Laboratory Data from an Earthquake History Study of Scarps in the Hanging Wall of the Tacoma Fault, Mason and Pierce Counties, Washington: U.S. Geological Survey Scientific Investigations Map 3060, 3 plates, includes interpretive text, http://pubs.er.usgs.gov/usgspubs/sim/sim3060.

Nelson, A.R., Personius, S.F., Sherrod, B.L., Kelsey, H.M., Johnson, S.Y., Bradley, L.-A., and Wells, R.E., 2014, Diverse rupture modes for surface-deforming upper-plate earthquakes in the southern Puget Lowland of Washington State: Geosphere, v. 10, no. 4, p. 769–796, doi:10.1130/GES00967.1.

Petersen, M.D., Frankel, A.D., Harmsen, S.C., Mueller, C.S., Haller, K.M., Wheeler, R.L., Wesson, R.L., Zeng, Y., Boyd, O.S., Perkins, D.M., Luco, N., Field, E.H., Wills, C.J., and Rukstales, K.S., 2008, Documentation for the 2008 Update of the United States National Seismic Hazard Maps: U.S. Geological Survey Open-File Report 2008–1128, 61 p.

Porter, S.C., and Swanson, T.W., 1998, Radiocarbon age constraints on rates of advance and retreat of the Puget lobe of the Cordilleran ice sheet during the last glaciation: Quaternary Research, v. 50, no. 3, p. 205–213, doi:10.1006/qres.1998.2004.

Puget Sound Power and Light Company (Puget Power), 1974, Preliminary Safety Analysis Report, Skagit Nuclear Project/Puget Power: Seattle, Washington, Puget Sound Power and Light Company, Volume 2, variously paginated.

Reimer, P.J., Baillie, M.G.L., Bard, E., Bayliss, A., Beck, J.W., Blackwell, P.G., Ramsey, C.B., Buck, C.E., Burr, G.S., Edwards, R.L., Friedrich, M., Grootes, P.M., Guilderson, T.P., Hajdas, I., Heaton, T.J., Hogg, A.G., Hughen, K.A., Kaiser, K.F., Kromer, B., McCormac,

F.G., Manning, S.W., Reimer, R.W., Richards, D.A., Southon, J.R., Talamo, S., Turney, C.S.M., van der Plicht, J., and Weyhenmeyer, C.E., 2009, IntCal09 and Marine09 radiocarbon age calibration curves, 0–50,000 years cal BP: Radiocarbon, v. 51, no. 4, p. 1111–1150.

Riedel, W., 1929, Zur Mechanik Geologischer Brucherscheinungen: Zentral-blatt fur Mineralogie: Geologie und Paleontologie, v. 1929B, p. 354–368.

Ryder, I., Rietbrock, A., Kelson, K., Burgmann, R., Floyd, M., Socquet, A., Vigny, C., and Carrizo, D., 2012, Large extensional aftershocks in the continental forearc triggered by the 2010 Maule earthquake, Chile: Geophysical Journal International, v. 188, p. 879–890, doi:10 .1111/j.1365-246X.2011.05321.x.

Ryves, D.B., Battarbee, R.W., Juggins, S., Fritz, S.C., and Anderson, N.J., 2006, Physical and chemical predictors of diatom dissolution in freshwater and saline lake sediments in North America and West Greenland: Limnology and Oceanography, v. 51, p. 1355–1368, doi:10 .4319/lo.2006.51.3.1355.

Sherrod, B.L., 2001, Evidence for earthquake-induced subsidence about 1100 years ago in coastal marshes of southern Puget Sound, Washington: Geological Society of America Bulletin, v. 113, no. 10, p. 1299–1311, doi:10 .1130/0016-7606(2001)113<1299:EFEISA>2.0.CO;2.

Sherrod, B.L., and Gomberg, J., 2014, Crustal earthquake triggering by prehistoric great earthquakes on subduction zone thrusts: Journal of Geophysical Research, v. 119, p. 1273–1294, doi:10.1002/2013JB010635.

Sherrod, B.L., Bucknam, R.C., and Leopold, E.B., 2000, Holocene relative sea level changes along the Seattle fault at Restoration Point, Washington: Quaternary Research, v. 54, p. 384–393, doi:10.1006/qres.2000.2180.

Sherrod, B.L., Brocher, T.M., Weaver, C.S., Bucknam, R.C., Blakely, R.J., Kelsey, H.M., Nelson, A.R., and Haugerud, R., 2004a, Holocene fault scarps near Tacoma, Washington, USA: Geology, v. 32, no. 1, p. 9–12, doi:10.1130 /G19914.1.

Sherrod, B.L., Nelson, A.R., Kelsey, H.M., Brocher, T.M., Blakely, R.J., Weaver, C.S., Rountree, N.K., Rhea, B.S., and Jackson, B.S., 2004b, The Catfish Lake Scarp, Allyn, Washington: Preliminary Field Data and Implications for Earthquake Hazards Posed by the Tacoma Fault: U.S. Geological Survey Open-File Report 2003-455, 14 p., 1 plate, http://pubs.usgs.gov/of/2003/of03-455/.

Sherrod, B.L., Blakely, R.J., Weaver, C.S., Kelsey, H.M., Barnett, E., Liberty, L., Meagher, K.L., and Pape, K., 2008, Finding concealed active faults: Extending the southern Whidbey Island fault across the Puget Lowland, Washington: Journal of Geophysical Research, v. 113, p. B05313, doi:10.1029/2007JB005060.

Sherrod, B.L., Barnett, E., Schermer, E., Kelsey, H.M., Hughes, J., Foit, F.F., Jr., Weaver, C.S., Haugerud, R., and Hyatt, T., 2013, Holocene tectonics and fault reactivation in the foothills of the north Cascade Mountains, Washington: Geosphere, v. 9, p. 827–852, doi:10.1130 /GES00880.1.

Spaulding, S.A., Lubinski, D.J., and Potapova, M., 2010, Diatoms of the United States: http://westerndiatoms .colorado.edu (accessed 14 April 2013).

Stirling, M., Rhoades, D., and Berryman, K., 2002, Comparison of earthquake scaling relations derived from data of the instrumental and preinstrumental era: Bulletin of the Seismological Society of America, v. 92, no. 2, p. 812–830, doi:10.1785/0120000221.

Sylvester, A.G., 1988, Strike-slip faults: Geological Society of America Bulletin, v. 100, p. 1666–1703, doi:10.1130 /0016-7606(1988)100<1666:SSF>2.3.CO;2.

Tabor, R.W., 1994, Late Mesozoic and possible Early Tertiary accretion in western Washington State—The Helena–Haystack mélange and the Darrington–Devils Mountain fault zone: Geological Society of America Bulletin, v. 106, no. 2, p. 217–232, 1 plate.

Tabor, R.W., Booth, D.B., Vance, J.A., and Ford, A.B., 2002, Geologic Map of the Sauk River 30- by 60-Minute Quadrangle, Washington: U.S. Geological Survey Geologic Investigations Series Map I-2592, 2 sheets, scale 1:100,000.

Tchalenko, J.S., 1968, The evolution of kink-bands and the development of compression textures in sheared clays: Tectonophysics, v. 6, no. 2, p. 159–174, doi:10.1016 /0040-1951(68)90017-6.

Tchalenko, J.S., 1970, Similarities between shear-zones of different magnitudes: Geological Society of America Bulletin, v. 81, p. 1625–1640, doi:10.1130/0016-7606 (1970)81[1625:SBSZOD]2.0.CO;2.

Troels-Smith, J., 1955, Characterization of Unconsolidated Sediments: Copenhagen, Denmark, Geological Survey of Denmark, Series IV, 73 p.

U.S. Geological Survey, 2013, Quaternary Fault and Fold Database of the United States: http://earthquake.usgs .gov/hazards/qfaults/ (accessed 2 May 2013).

Van Wagoner, T.M., Crosson, R.S., Creager, K.C., Medema, G.F., Preston, L.A., Symons, N.P., and Brocher, T.M., 2002, Crustal structure and relocated earthquakes in the Puget Lowland, Washington, from high-resolution seismic tomography: Journal of Geophysical Research, v. 107, no. B12, 2381, p. ESE 22-1–22-23, doi:10.1029 / 20012JB000710.

Walsh, T.J., and Logan, R.L., 2007, Field Data for a Trench on the Canyon River Fault, Southeast Olympic Mountains, Washington: Washington Division of Geology and Earth Resources Open-File Report 2007-1, 1 sheet.

Washington Division of Geology and Earth Resources, 2010, Digital Geology of Washington State at 1:100,000 Scale, Version 3.0: http://www.dnr.wa.gov/ResearchScience /Topics/GeosciencesData/Pages/gis_data.aspx (accessed on 20 December 2013).

Wells, D.L., and Coppersmith, K.J., 1994, New empirical relationships among magnitude, rupture length, rupture width, rupture area and surface displacement: Bulletin of the Seismological Society of America, v. 84, p. 974–1002.

Wells, R.E., and McCaffrey, R., 2013, Steady rotation of the Cascade arc: Geology, v. 41, p. 1027–1030, doi:10 .1130/G34514.1.

Wells, R.E., and Simpson, R.W., 2001, Northward migration of the Cascadia forearc in the northwestern U.S. and implications for subduction deformation: Earth, Planets, and Space, v. 53, no. 4, p. 275–283, doi:10.1186 /BF03352384.

Wells, R.E., Weaver, C.S., and Blakely, R.J., 1998, Forearc migration in Cascadia and its neotectonic significance: Geology, v. 26, p. 759–762, doi:10.1130/0091-7613 (1998)026<0759:FAMICA>2.3.CO;2.

Wells, R., Bukry, D., Friedman, R., Pyle, D., Duncan, R., Haeussler, P., and Wooden, J., 2014, Geologic history of Siletzia, a large igneous province in the Oregon and Washington Coast Range: Correlation to the geomagnetic polarity time scale and implications for a long-lived Yellowstone hotspot: Geosphere, v. 10, p. 692–719, doi:10.1130/GES01018.1.

Wesnousky, S.G., 2008, Displacement and geometrical characteristics of earthquake surface ruptures: Issues and implications for seismic hazard analysis and the process of earthquake rupture: Bulletin of the Seismological Society of America, v. 98, no. 4, p. 1609–1632, doi: 10.1785/0120070111.

Whetten, J.T., Carroll, P.I., Gower, H.D., Brown, E.H., and Pessl, F., Jr., 1988, Bedrock Geologic Map of the Port Townsend 30- by 60-Minute Quadrangle, Puget Sound Region, Washington: U.S. Geological Survey Miscellaneous Investigations Series Map I-1198-G, scale 1:100,000, 1 sheet.

Wilson, J.R., Bartholomew, M.J., and Carson, R.J., 1979, Late Quaternary faults and their relationship to tectonism in the Olympic Peninsula, Washington: Geology, v. 7, no. 5, p. 235–239, doi:10.1130/ 0091–7613 (1979)7<235:LQFATR>2.0.CO;2.

Witter, R.C., Givler, R.W., and Carson, R.J., 2008, Two postglacial earthquakes on the Saddle Mountain West fault, southeastern Olympic Peninsula, Washington: Bulletin of the Seismological Society of America, v. 98, no. 6, p. 2894–2917, doi:10.1785/0120080127.

Zdanowicz, C.M., Zielinski, G.A., and Germani, M.S., 1999, Mount Mazama eruption: Calendrical age verified and atmospheric impact assessed: Geology, v. 27, p. 621–624, doi:10.1130/0091-7613(1999)027<0621: MMECAV>2.3.CO;2.

Zollweg, J.E., and Johnson, P.A., 1989, The Darrington seismic zone of northwestern Washington: Bulletin of the Seismological Society of America, v. 79, no. 6, p. 1833–1845.